

Batch and continuous fixed-bed column adsorption of Cd(II) from aqueous solution and industrial effluent by functionalized nano-structured cellulose particles

Azeh Yakubu^{a,*}, Folahan Amoo Adekola^b, Gabriel Ademola Olatunji^b

^aDepartment of Chemistry, Ibrahim Badamasi Babangida University, Lapai, Niger State, Nigeria, email: yakubuazeh@gmail.com

^bDepartment of Industrial Chemistry, University of Ilorin, Ilorin, Nigeria, emails: faadekola@yahoo.fr (F.A. Adekola), m_ade49@yahoo.com (G.A. Olatunji)

Received 15 August 2018; Accepted 2 May 2019

ABSTRACT

Adsorption of cadmium (II) has been investigated on phosphorylated and functionalized nanocelluloses (azeh2, azeh10 and azeh-TDI). The results demonstrated the capacity of the nanoparticles to reduce Cd(II) in aqueous solution. The performance of the nanocellulose varied accordingly azeh2 > azeh-TDI > azeh10. 53%–99% removal ratio was achieved and adsorption was pH dependent with the best performance of 0.4 g/L. The sorption process was exothermic for azeh2 and azeh10 whereas it was endothermic for azeh-TDI sample. Sorption of Cd(II) was best fitted by the pseudo-second-order kinetics model. Low ionic strength favoured the adsorption of Cd(II), with the best desorption of metal-loaded cellulose nanoparticles achieved at high concentration of HNO₃. Desorption kinetics data fitted the Elovich kinetics. Fixed-bed column adsorption of Cd(II) demonstrated the ability of the nanocelluloses to adsorb Cd(II) in the effluent from the nail and roofing sheet making industry. The 6 cm bed depth adsorbed 0.019–2.740 mg/g of Cd(II) while 8 cm bed depth adsorbed 0.016–2.301 mg/g of Cd(II), respectively. Sorption kinetics was Thomas and Yoon–Nelson model. Packed column reduced 2,000 to 30 cfu/mL microbial contaminants after 24 h of treatment in the column. The nanocelluloses are promising bioadsorbent for treatment of water/wastewater system laden with metals and microbes.

Keywords: Adsorption; Nanocelluloses; Cd(II); Batch; Column

1. Introduction

Environmental pollution and its harmful effect on ecology have been studied and reviewed intensively by different research groups [1–5]. Problems of the pollutants removal from wastewater were increased with rapid development of industries such as metal plating facilities, mining operations, fertilizer industries, tanneries, batteries, paper industries and pesticides, etc., heavy metals wastewaters are directly or indirectly discharged into the environment

increasingly, especially in developing countries [1–3,6–11]. Unlike organic contaminants, heavy metals are not biodegradable and tend to accumulate in all forms of life and many heavy metal ions are known to exhibit lethal effects on living organisms even at low concentration [3,6–12]. Toxic heavy metals of particular concern in treatment of industrial wastewaters include zinc, copper, nickel, mercury, cadmium, lead and chromium, iron, selenium, vanadium and cobalt [2,6,7,11]. These heavy metals are of specific concern due to their toxicity, bio-accumulation tendency and

* Corresponding author.

persistency in nature [6]. Various methods are being used for the removal of heavy metals and they include chemical or electrochemical precipitation, ion-exchange, complexation, solvent extraction, evaporation, oxidation and reduction, which do not appear to be economical [3,7,9,12]. Different low-cost bio-adsorbent materials with different adsorption capacities for different heavy metals have been reported by various researchers [2,6,7]. The application of nanocellulose materials for water filtration is a novel and emerging area. The largest potential volume of cellulose nanomaterial application are paper and paper packaging, textiles, cement, and automobile parts, while smaller volume applications include sensors, construction, aerospace materials, cosmetics, pharmaceuticals and paint additives [11].

Cellulose constitutes the most abundant and renewable polymer resource available worldwide and comprises of repeating 1-4-D-glucopyranose units covalently linked through acetal functions between the OH groups of C4 and C1 carbon atoms providing it hydrophilicity, chirality and reactivity properties [3,10,13]. Modified cellulose materials have been used for heavy metal removal in various water/wastewater systems and their results showed different adsorption capacities depending on the type of adsorbent used [3]. Increasing interests in the use of nanomaterials of plant origin has led to intensive research in the area of nanocelluloses, as a result of its unique properties and natural abundance, biodegradable, biocompatible and its renewability have made it suitable for environmental and health applications [13]. Recently, a composite material has been used for removal of Cd(II) [14]. Heavy metal adsorbents based on amidoximated-grafted-cellulose and regenerated cellulose wood pulp grafted with the vinyl monomer glycidyl methacrylate (GMA) cellulose-g-GMA-imidazole copolymer material have been investigated with respect to the adsorption of Pb(II), Cd(II), Zn(II) Fe(II), Cu(II), Ni(II) and Co(II) from aqueous solution [15,16]. Magnetic cellulose-chitosan hydrogels adsorbent for the remediation heavy metals from aqueous solutions have been synthesized from ionic liquids [17]. Recently, a novel metal adsorbent based on grafted amino-terminated hyperbranched polymer (HBP-NH₂) onto bagasse cellulose was used for the adsorption of Cr(VI) ions in aqueous solutions [18]. However, not much attention has been paid on the application of phosphorylated nanocelluloses fibres/crystals/particles for the remediation of toxic metals from water bodies/waste effluents. As a biopolymer, cellulose is a cheaper alternative adsorbent material with promising potentials for regeneration compared with synthetic adsorbents.

2. Experimental work

2.1. Materials and methods

All the chemicals used for the synthesis of nanocellulose and its derivatives were of analytical grade and obtained from BDH Chemicals Ltd., (Poole, England). They were used without any further purification and these include cellulose and H₃PO₄, Cd(NO₃)₂, HNO₃, NaOH were obtained from BDH Chemicals. Toluene diisocyanate (TDI) was obtained as a gift from Vita Plc Oba-akran Avenue, Ikeja, Lagos, Nigeria and was used as provided.

2.2. Synthesis and purification of cellulosic nanocrystals

The preparation of cellulose nanocrystals followed the procedures described by Filpponen [19], Rosa et al. [20], Azeh et al. [21]. In a typical experiment, 1 g of each cellulosic source material was hydrolyzed using 40 mL 64% (4.57 mL/g) concentrated H₂SO₄, HCl and H₃PO₄ (analytical grade) at 50°C for 3/6 h under continuous mechanical stirring with a Teflon-coated magnetic bar. The resulting suspension obtained had different colours depending on hydrolysis time. The obtained viscous suspension was neutralized using distilled water and then centrifuged at 3,000 rpm for 30 min. and then washing was repeatedly carried out using centrifugation until the nanoparticle obtained was neutral. The thoroughly washed products were then kept in suspension by the addition of deionized water in plastic sample bottles and then stored in a refrigerator. These samples were used for Fourier transform infrared (FT-IR), scanning electron microscope (SEM), X-ray diffraction crystallography, thermogravimetry analysis (TGA), differential thermogravimetry analysis (DTGA) and Brunauer-Emmett-Teller (BET) analysis. Soluble products obtained were allowed to stand to precipitate overnight.

2.3. Modification using toluene diisocyanate

The modification of cellulose nanoparticles (phosphonated-cellulose nanoparticles (azeh2) or phosphonated cellulose acetate nanoparticles (azeh10) was carried out by reacting 1.62 g (10 mmol) of the celluloses with 1.72 g (10 mmol) of toluene diisocyanate (TDI) in 50 mL of toluene in the presence of triethylamine as catalyst for the diisocyanate reaction. The mixture in a round bottom flask was placed on a magnetic stirrer and was stirred at 90°C for 24 h using Teflon coated magnetic bar. After this, the mixture was filtered and the yellowish residue obtained was washed with ethanol followed by deionized water and then air dried [22]. This was used for further analysis.

2.4. Preparation of cadmium (II) stock solutions

Stock solutions of 1,000 mg/L were prepared by dissolving appropriate amounts of Cd(II) nitrate salt in distilled-deionized water. Adjustment of pH was accomplished using 0.1 M NaOH or 0.1 M HNO₃ to obtain test solutions with pH values ranging from 2 to 10 [8].

2.5. Equilibrium adsorption experiment

The adsorption of Cd(II) ions by azeh2 and azeh10 was investigated by batch adsorption. The effect of contact time for 240 min, solution pH (2–10), adsorbent dosage (0.4–1.2 g), solution temperature (293–333 K) and initial concentration (1–10 mg/L) on the adsorption were investigated [8].

2.6. Adsorption studies

2.6.1. Adsorption of Cd(II) on the synthesized nanocellulose materials

2.6.1.1. Effect of initial metal ion concentration

The synthesized samples (0.2 g) were weighed using an analytical balance and were contacted with 20 mL of an initial

Cd(II) concentration of 1–10 mg/L and equilibrated on an orbital shaker for 240 min at 298 K. The mixture was filtered and analyzed on an atomic absorption spectrophotometer (AAS) (iCE 3000 AA02134104 v1.30 model). Absorption capacity of Cd(II) ions were measured and calculated from the difference between the initial and final concentrations of Cd [10]. The amount adsorbed (mg/g) was calculated using the formula:

$$Q = (C_i - C_f) \times \frac{V}{W} \quad (1)$$

where Q = quantity of solute adsorbed from solution of volume, V (L); C_i = initial concentration before adsorption; C_f = concentration after adsorption; V = volume of adsorbate used, L; W = mass of the adsorbent, g.

2.6.1.2. Effect of pH

The effect of pH was carried out by varying the pH 2–10 of the 20 mL 3 mg/L Cd(II) solution from 2 to 10 using 0.1 M NaOH or 0.1 M HNO₃ to monitor the pH of the metal solutions.

2.6.1.3. Effect of adsorbent dosage

This was carried out by using constant adsorbate of 20 mL 3 mg/L Cd(II) solution with adjusted pH to the optimal pH 4. azeH2 and azeH10 of dosage (0.4–1.2 g) was mixed with the metal solution in a 100 mL flask and the mixture was shaken for 120 min. The mixture was filtered and analyzed for residual Cd(II) ions in the filtrate by atomic absorption spectrophotometer.

3. Results and discussion

3.1. Scanning electron microscopy

The SEM images revealed the morphology of the synthesized nanoparticles with various irregular shapes ranging from rod-like to single and agglomerated crystals. Particles with diameter in the range of 68–843 nm were

obtained. BET surface areas of the nanocelluloses prepared were 105.698 and 250.570 m²/g, whereas, the pore size ranged from 1.324 to 9.237 nm with pore volume in the range of 0.01427–0.07939 cm³/g, respectively [21].

3.2. Thermogravimetry analysis

TGA of the synthesized nanoparticles showed that at T_{95} and T_{90} (mass loss), the degradation temperature of the prepared nanocelluloses was in the range of 297.51°C–411.09°C and 315°C–508.55°C while the maximum (T_{max}) degradation temperature ranged from 375°C to 525°C [21].

3.3. Effect of initial ion concentration

The equilibrium adsorption of Cd(II) ion on azeH2 sample was investigated by equilibrating 20 mL of simulated aqueous Cd(II) solution of different concentrations ranging from 1 to 10 mg/L with 0.2 g of the adsorbent at a pH of 4.0 at 300 K for 240 min. The initial metal ion concentration in solution is an important factor that can influence adsorption behaviours of the adsorbent. The amount of Cd(II) ion adsorbed increased with increasing metal ion concentration and reached a maximum at 10 mg/L. This was attributed to the available active site on the adsorbent surface. The results of this investigation showed that appreciable amount of Cd(II) ions can be removed by the sample in the range of 3–10 mg/L of initial concentration. The azeH2 sample showed 3.30%–71.62% efficiency to remove Cd(II) ions in aqueous solution. This confirms that increase in concentration is proportional to increase in the number of particles in solution similar to the findings in the literature [2,8,10,12,19]. Furthermore, the large surface area, micropore volume, surface charge coupled with the size of the nanoparticles and the presence of metal scavenging oxygen atoms of the phosphate ester on the surface of the nanoparticles also played significant roles in the adsorption of Cd similar to our previous report on the adsorption of Pb by the cellulose nanomaterials [8]. Similarities in the surface charge of the particles could bring about electrostatic repulsion that could lead to the existence of the nanoparticles as individual particles, may also have positive influence on the adsorption of Cd as earlier reported by AzeH et al. [8].

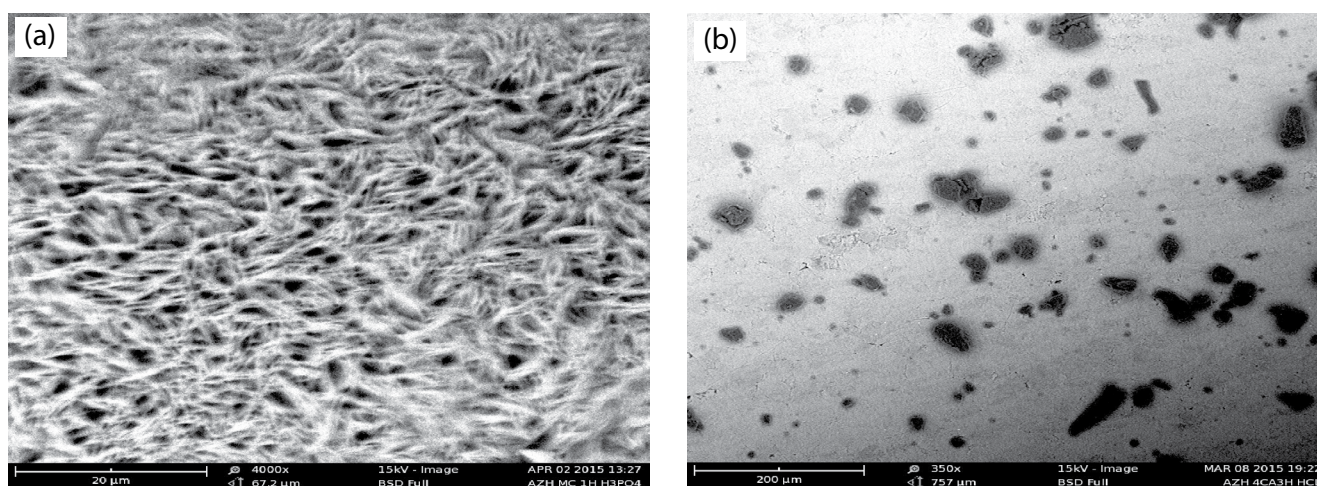


Fig. 1. SEM image of nanoparticles adopted [21].

A report on the use of agricultural waste for the sorption of Pb^{2+} and Cd^{2+} with the maximum uptake of Cd in the range of 5.1–52.2 mg/g have been documented [23]. The presence of hydroxyl ($-OH$), phosphonic ($-OPO_3H_2$ and $-OPO_3^{2-}$), sulphate ($-SO_3^{2-}$, and carbonyl ($C=O$) groups have been reported as potential metal scavenging sites on the cellulose nanomaterials [8,11]. The presence of these groups was revealed by the FT-IR results of the samples [21]. Moreover, sulphonic groups on the surface of the synthesized nanocellulose are likely to have a greater degree of ionization at higher pH than the other functional groups in cellulose (hydroxyl or carboxyl groups), so that the electrostatic affinity of the sulphonic group for the metal ions may be stronger and hence, increase in the metal uptake was observed similar to our previous findings on Pb adsorption by phosphorylated nanocellulose (azeh2), cellulose acetate (azeh10) and cellulose-carbamate (azeh-TDI) [8] and the findings by Liu [24] on the removal of Ag(I), Fe(III) and Cu(II) ions by phosphorylated nanocellulose. Functionalized nanocelluloses have shown to have high adsorption capacities for metal ions than their native counterpart based on the functional surface [24–27].

3.4. Adsorption kinetics

3.4.1. Effect of contact time on adsorption of Cd(II) ions

Contact time is an important factor investigated in the evaluation of the efficiency of adsorbents in adsorption studies, as it helps in revealing the rate of maximum removal of adsorbate in solution. The effect of contact time on Cd(II) ion in aqueous solution is represented in Fig. 2. The adsorption of Cd(II) ion by azeh2, azeh10 and azeh-TDI occurred rapidly within the first 10–30 min of adsorption, followed by equilibrium attainment at 360 min (Fig. 2). The amount of Cd(II) removed by azeh-TDI sample within the 10–30 min of contact time was in the range of 0.1014–0.2005 mg/g, representing 38%. After this the adsorption increased and reached a maximum at 360 min, where 58%, 78% and 78% adsorption capacity were achieved on Cd(II) adsorption onto azeh10, azeh2 and azeh-TDI, respectively. After 360 min the adsorption rate of Cd(II) ions stabilized considerably (equilibrium point). The increase in the time from 30 to 360 min led to an increase of 20% to 40% in Cd(II)

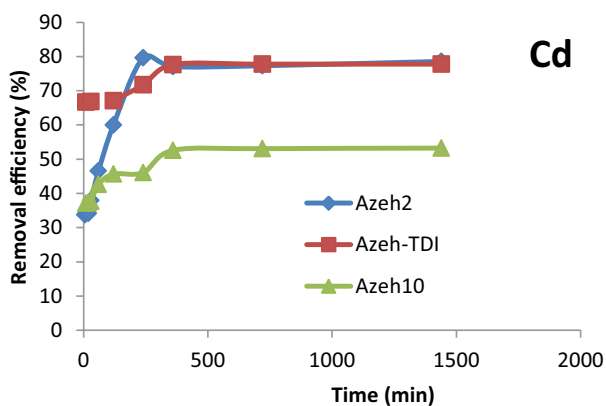


Fig. 2. Effect of contact time on removal efficiency of Cd(II) by Azeh2, Azeh-TDI and Azeh10 at equilibrium concentration.

adsorption capacity at 360 min. This was attributed to N–H, C–N and C=O groups as metal chelating sites on the surface of the modified samples bearing these groups ($3,340$ – $3,280$ and $1,590$ cm^{-1} for N–H) and ($1,220$ and $1,650$ cm^{-1} for C–N and C=O stretching vibration) [8,22]. There are similarities in the adsorption of Cd(II) onto the nanocelluloses, due probably to the similarities in their surface functionalities. This is in agreement with the findings by Lim et al. [25] and Suopajarvi [28] on the adsorption of Cd(II) ion in aqueous solution by cellulose nanoparticles and nanofibres. The maximum adsorption capacity for Cd(II) removal in aqueous solution within the 24 h of agitation were 0.2357, 0.1597 and 0.2333 mg/g while the adsorption efficiency was in the range of 58%–78% with azeh2 and azeh-TDI having the highest adsorption capacity of 78%.

Generally, the adsorbents showed high abilities to remove Cd(II) in aqueous solution, irrespective of differences in their functional surfaces. The $-PO_3^{2-}$ group has been found to have high metal-binding abilities [21]. In our previous study, we reported that the adsorption of Pb(II) onto the cellulose nanoparticles was influenced by the presence of functional groups such as P–O, P–O–C, P–OH (900 – $1,003$ cm^{-1}) and the P=O, peak at $1,203$ cm^{-1} [8,22]. High adsorption values obtained in this work could be due to the high negative charge density and the absence of agglomeration during agitation similar to the findings by Lim et al. [25] on the adsorption of Fe(III), Ag(I) and Cu(II) onto Phos-CNC and Phos-CNF and polyfunctional acids (citric, tartaric and phosphoric) treated agricultural materials [26]. Furthermore, the adsorption process is assumed to be a cation exchange tendency of the phosphonic group ($-OPO_3H_2$) on the surface of the nanocelluloses for H^+/Na^+ ions in solution. The phosphonic group ($-OPO_3H_2$) has been found with high affinity and selectivity towards Cd(II) ion in solution because of the wide pH range that strong acid cation exchangers dissociate [29,30]. The adsorption process was due to chemical reactions between the adsorbate ions in solution and active functional species on the surface of the adsorbents [31,32] as it favours the Langmuir model.

3.4.2. Effect of sample dose on the adsorption behaviours of Cd(II) ions

The results of the adsorbent dose are presented in Fig. 3. Varying amounts of the adsorbents over an adsorbent dose of 0.4–1.2 g/L were used. The results show that the sample surface area, pore volume, size and the chemical functionalities on the surface of the adsorbents influenced the adsorption of Cd(II). Small amount showed high adsorption similar to the reports by Adegoke et al. [10] and Lim et al. [25] on synthetic hematite nanoparticles and nanocellulose. The large radius of Cd(II) (0.426 nm) and its low electronegativity (1.69) may affect the adsorption of Cd(II) ion in solution. The maximum capacity and removal efficiency of sample azeh2 (cellulose nanoparticles) and azeh10 (cellulose acetate nanoparticles) were 0.0995 and 0.140 mg/g, representing 65.30% and 65.30%, respectively.

3.4.3. Effect of temperature on adsorption of Cd(II) ions

The result of the experiments on solution temperature is presented in Fig. 4. Sample azeh2 showed an increase in

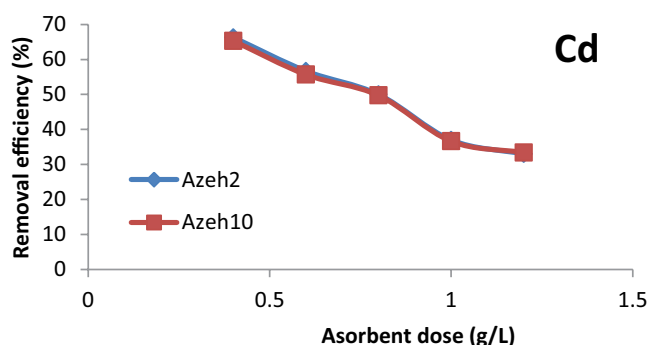


Fig. 3. Effect of adsorbent dose on removal efficiency of Cd(II) ion onto Azeh2 and Azeh10 at equilibrium concentration.

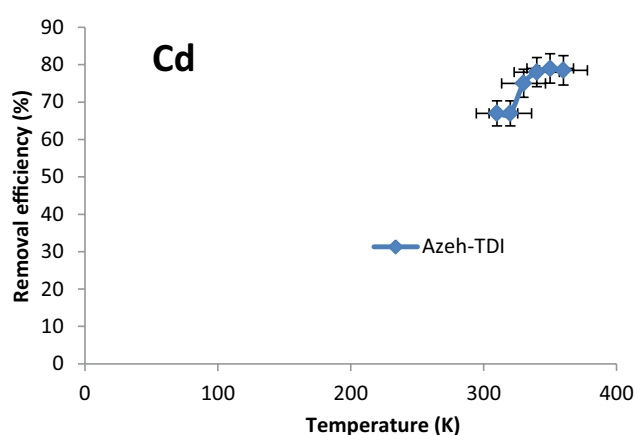


Fig. 4. Effect of temperature on removal efficiency of azeH-TDI on Cd(II) ions in solution at equilibrium concentration.

the amount Cd(II) adsorbed from 300–320 K. After 320 K, no further increase in the adsorption of Cd(II) was recorded with raising the temperature to 320 K. However, for the sample azeH10, the effect of temperature was not observed. The maximum adsorption capacities were 0.2999 mg/g, corresponding to 79% efficiency. The solution temperature had significant influence on the adsorption of Cd(II) onto cellulose nanomaterials, where the samples showed improved adsorption capacity and removal efficiency. Sample azeH-TDI exhibited a different adsorption pattern, where the adsorption capacity increased with increasing solution temperature up to 350 K, where 67%, 67%, 75%, 78%, and 79% adsorption of Cd(II) was achieved. After 350 K, adsorption gradually stabilized.

3.4.4. Effect of pH on adsorption of Cd(II) ions in aqueous solution

Solution pH is one of the important parameter governing the removal of metal ions from aqueous solutions as it has significant effect on the adsorbent surface charge and the degree of ionization [7,10,12,28]. When the pH of the adsorbing medium is from 1 to 5 (acidic), divalent Cd(II) ions are predominantly the species in solution, where there is complete absence of precipitation/nucleation processes while at $\text{pH} > 8$ (alkaline), there is the likelihood of the

precipitation/formation of hydroxylated $[\text{Cd}(\text{OH})_2]$ forms of Cd(II) in solution, where the removal of Cd(II) is a combination of adsorption and precipitation [33,34]. Fig. 5 shows the adsorption behaviours of the synthesized nanomaterials as a function of change in pH. It was observed that adsorption capacities for Cd(II) removal onto azeH2 and azeH10 increased with increasing pH and reaches a maximum at pH 4, where the adsorbents exhibited highest adsorption capacity of 0.210 and 0.2898 mg/g, representing 99.47% and 99.47%. At this pH, Cd(II) species are sufficiently soluble and available for the adsorption sites on the cellulose adsorbents. The maximum adsorption at pH4 may be attributed to deprotonation of hydrogen ions in solution due to increase in the pH and the high negative charge surface of the cellulose nanomaterials. This was attributed to repulsion between the negatively charged hydroxylated species on the adsorbent surface and saturation of the active sites similar to the findings by AzeH et al. [8] and Mautner et al. [35]. The occupation of the binding sites on the adsorbent surface by metal ions may also contribute to decrease in adsorption. The above reasons may also be justified by the values of the $\text{pH}_{\text{pzc}} = 1.79$ and 1.50 for sample azeH2 and azeH10 as reported by AzeH et al. [8]. The performance of the cellulose nanomaterials was pH dependent, where both samples showed high removal ratio for Cd(II) at $\text{pH} = 4$ [8,28,36]. The results of this study agreed with the findings by Gurgel and Gil [37]. The low electronegativity of Cd(II) and its large hydrated radius probably caused a decrease in the adsorption capacity [34].

3.5. Adsorption isotherm, kinetics and thermodynamic models

3.5.1. Adsorption isotherms

The adsorption isotherm, kinetics and thermodynamic models for Cd(II) ions removal by three different synthesized nanomaterials (azeH2, azeH10 and azeH-TDI) were fitted with Langmuir (Figs. 6–8), Freundlich (Figs. 9–11), Temkin (Figs. 12–14) and Dubinin–Radushkevich (D-R) isotherm models and kinetics, intraparticle diffusion, power function and Elovich models in order to determine the models that described best the adsorption process for Cd(II) ions.

3.5.2. Langmuir isotherm, Freundlich, Temkin and Dubinin–Radushkevich (D-R)

Parameters for the four models (Langmuir, Freundlich, Temkin and D-R isotherm) used to describe the sorption of Cd(II) ions by azeH2, azeH10 and azeH-TDI are presented in Table 1. As it can be seen in Table 1 that for azeH2, azeH10 and azeH-TDI, the maximum monolayer adsorption capacity (q_m) of 0.081, 0.060 and 0.1563 mg/g obtained for 0.2 g, adsorbent dose, respectively, and these are less than the corresponding experimental adsorption capacity (q_{exp}). It means that the maximum monolayer adsorption capacity (q_m) obtained from the experimental data based on Langmuir isotherm model was less than the experimental adsorption capacity, indicating that the maximum amount of Cd(II) ions monolayer coverage on a unit mass of the nanomaterials was exceeded by the experimental value (q_{exp}); hence the adsorption process deviated from the Langmuir

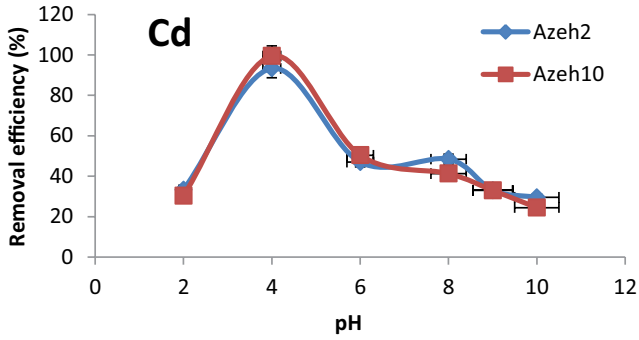


Fig. 5. Effect of pH on removal efficiency of Cd(II) adsorption onto aze2 and aze10 at equilibrium concentration.

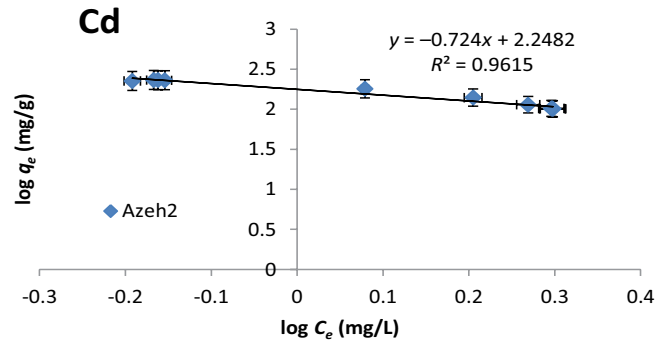


Fig. 9. Freundlich isotherm plot aze2.

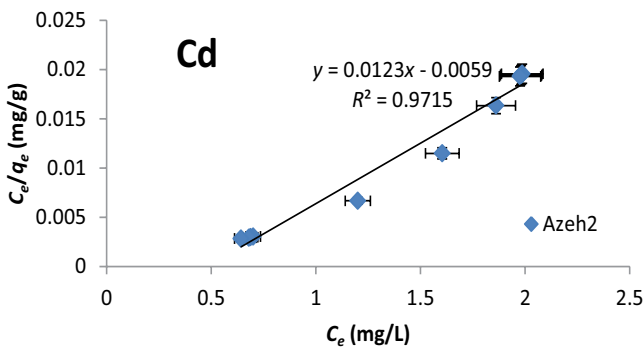


Fig. 6. Langmuir isotherm plot aze2.

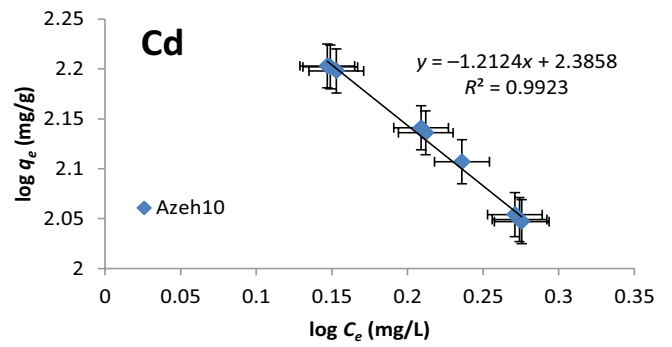


Fig. 10. Freundlich isotherm plot aze10.

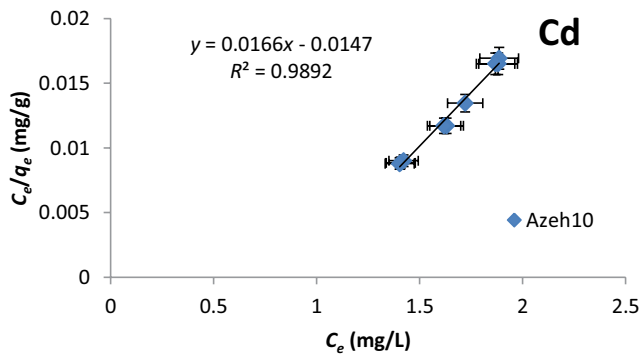


Fig. 7. Langmuir isotherm plot aze10.

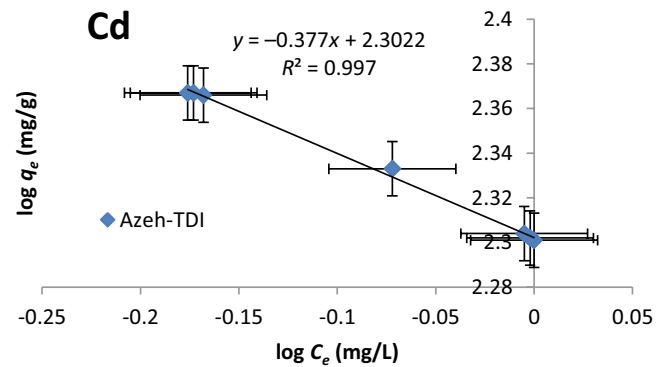


Fig. 11. Freundlich isotherm plot azeh-TDI.

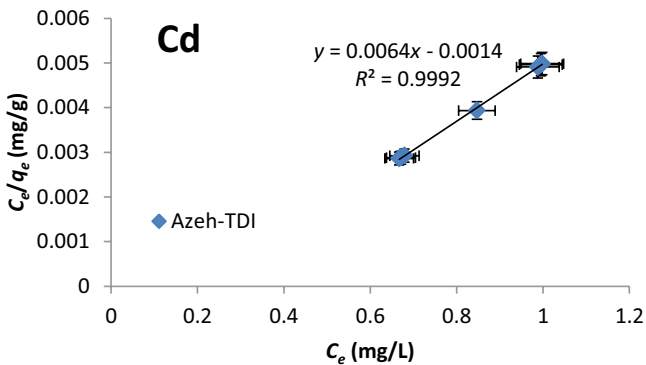


Fig. 8. Langmuir isotherm plot azeh-TDI.

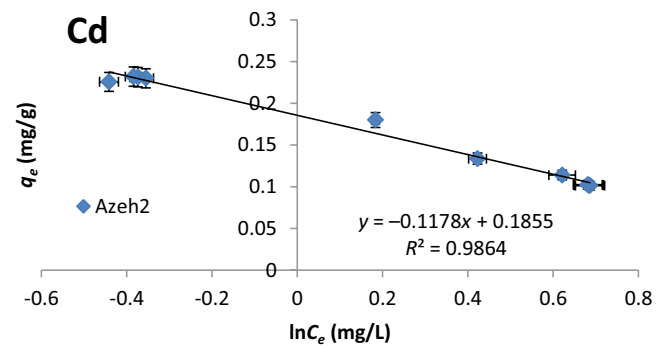


Fig. 12. Temkin isotherm plot aze2.

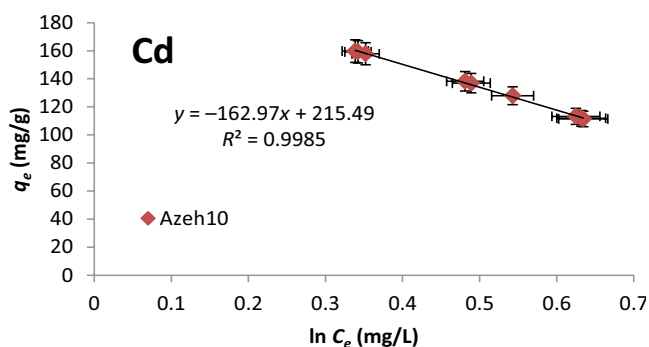


Fig. 13. Temkin isotherm plot azeh10.

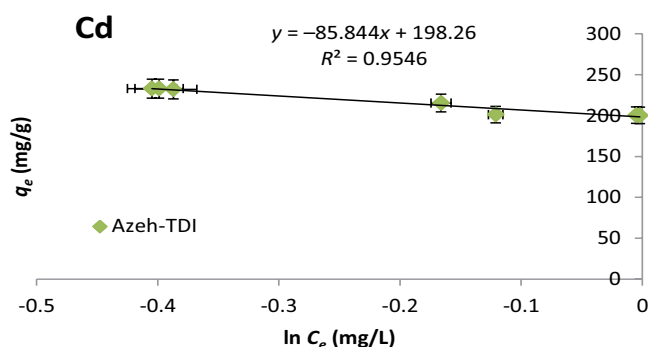


Fig. 14. Temkin isotherm plot azeh-TDI.

Table 1
Adsorption isotherm constants and the Chi-square (χ^2) calculated for Cd(II) adsorption

Adsorbents	Langmuir coefficients					Freundlich coefficients				Temkin coefficients			
	q_m	$-b$	R_L	R^2	χ^2	n	K_f	R^2	χ^2	b	K_T	R^2	χ^2
Azeh2	0.081	0.478	-2.31	0.972	0.091	-1.38	0.1771	0.9615	0.009	-21.29	0.2045	0.9861	0.007
Azeh10	0.060	0.886	-0.60	0.989	0.059	-0.83	0.2431	0.9923	0.063	-15.31	0.2665	0.9985	0.081
Azeh-TDI	0.1563	0.219	2.91	0.999	0.024	-2.65	0.2005	0.9970	0.002	29.06	10.07	0.9546	9.649

assumption. Values of q_m for Cd(II) showed similar trend for Cd(II) adsorption onto azeh2, azeh10 and azeh-TDI. The order of q_m is azeh-TDI > azeh2 > azeh10. The above trend as shown by the values of q_m suggests the existence of a multilayer adsorption phenomenon. From the isotherm results of Cd(II) sorption, the goodness of fit for the synthesized cellulose nanomaterials for each sample by three different isotherm models was in the order; Temkin > Langmuir > Freundlich – 0.9861 > 0.972 > 0.9615 for azeh2; Temkin > Freundlich > Langmuir – 0.9985 > 0.9923 > 0.989 for azeh10, and Langmuir > Freundlich > Temkin – 0.999 > 0.9970 > 0.9546 for azeh-TDI (Figs. 6–14), respectively. Generally, the goodness of fit for the sorption isotherms of Cd(II) showed consistency in their R^2 values similar to the findings on Pb(II) adsorption by Azeh et al. [8]. The isotherm that described best the adsorption of Cd(II) was Freundlich isotherm model which showed high K_f values, indicative of the high adsorption capacity and intensity of the nanomaterials. The K_f values of azeh10 and azeh-TDI were higher than H_3PO_4 acid modified sample (azeh2). While the value of n , which suggests the distribution of bonded ions was negative for the three adsorbents. This indicates unfavourable adsorption [37]. The Temkin equation showed good correlation coefficient (R^2) for the adsorption of Cd(II) ions, which implies that it could be used to describe the sorption of Cd(II) by the adsorbents. The separation factor from the Langmuir isotherm model, indicative of the affinity between adsorbate and adsorbent surface, (R_L) calculated for Cd(II) ions sorption process were -2.31 and -0.60 for azeh2 and azeh10, respectively. The R_L values are less than 1, and indicates high favourability of the model for Cd(II)-azeh2 and Cd(II)-azeh10. It also implies that Cd(II) ions prefer to remain bound to the surface of the sample similar to Pb(II) ions [8]. The R_L value for azeh-TDI sample was 2.91. This value is

greater than one and it confirmed the unfavourability of the Langmuir isotherm. This was in contrast to the adsorption of Pb by these samples [8]. The energy of sorption described by Temkin model (b) and (K_T) was in the range of 11.4–13.4 and 0.4686–15.42 J/mol for the sorption of Cd(II). This model also described the adsorption process well based on the correlation coefficient (R^2) in decreasing order accordingly; 0.9985-azeh10 > 0.9861-azeh2 > 0.9546-azeh-TDI.

The Dubinin–Radushkevich isotherm model (Figs. 15–18) was used in order to estimate the characteristics porosity of the synthesized nanomaterials and the apparent energy of sorption of Cd(II). The model is represented as follows:

$$q_e = q_s \exp \left(-B \left[RT \ln \left(1 + \frac{1}{C_{eq}} \right) \right]^2 \right) \quad (2)$$

where B is related to the free energy of sorption per molecule of sorbate as it migrates from the bulk solution to the surface of the adsorbent from infinite distance, calculated as [38] follows:

$$E = \frac{1}{(2B)^{\frac{1}{2}}} \quad (3)$$

q_s is the Dubinin–Radushkevich isotherm constant related to the degree of sorbate sorption by the sorbent surface. The linear form of the equation is given as:

$$\ln q_e = \ln q_s - 2BRT \ln \left(1 + \frac{1}{C_e} \right) \quad (4)$$

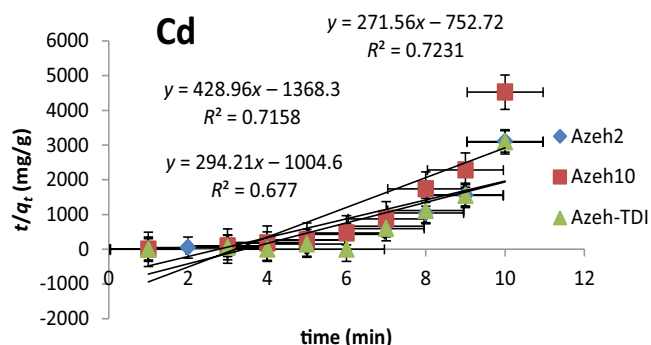


Fig. 15. Pseudo-second order kinetics plot aze2, aze10 and aze-TDI.

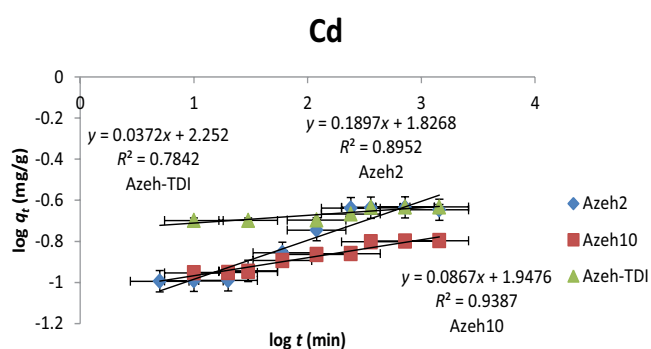


Fig. 16. Power function kinetic plot aze2, aze10 and aze-TDI.

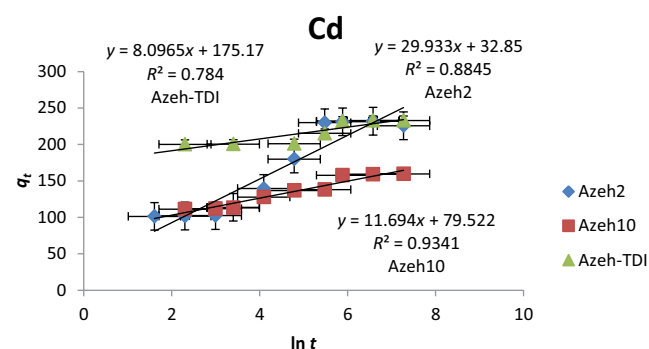


Fig. 17. Elovich plot.

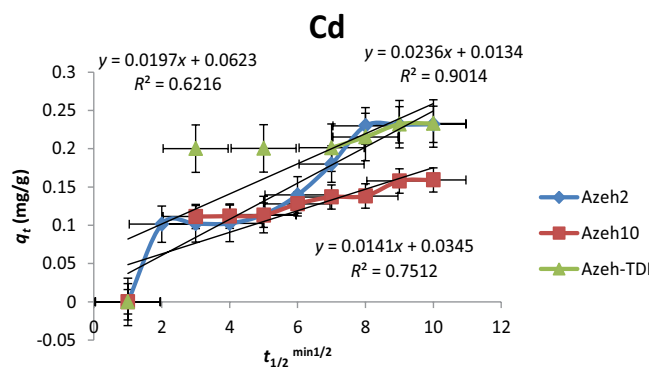


Fig. 18. Intraparticle diffusion plot.

The plots of $\ln q_e$ against

$$RT \ln \left(1 + \frac{1}{C_e} \right) \quad (5)$$

yield straight lines and indicates a good fit of the isotherm to the experimental data based on the R^2 .

The linear regression values of q_s and B calculated from the intercepts and slopes of the plots and apparent energy (E) of adsorption are shown in Table 2.

Increase in the values of q_e was observed. This was an indication of high adsorption capacity of the adsorbents. The values of q_s (Table 2) ranged from 0.2215 to 0.3577 mg/g for the three adsorbents. The sample coded as aze-TDI exhibited the highest sorption capacity than aze2 and aze10. This was linked to the new functionalities on the surface of the adsorbent due to chemical modification. The values of the apparent energy of Cd(II) adsorption (Table 2) depicts a physisorption process similar to the findings by Azeh et al. [8] and Itodo et al. [38]. This means that the Dubinin–Radushkevich isotherm can be used to describe the adsorption of Cd(II) on the nanomaterials. The mean free energy of adsorption of Cd(II) ions by the nanomaterials was positive. This indicates that an endothermic process was favoured and high positive values indicate that the adsorption process corresponds to ion exchange process similar to the findings by Azeh et al. [8], and Yakout and Elsharif [39].

The coefficients of regression (R^2) of the four isotherms were compared as shown in Table 3. The R^2 for the Langmuir isotherm (Figs. 6–8) ranged from 0.972 to 0.999 with an average value of 0.9867. The Freundlich isotherm (Figs. 9–11), R^2 ranged from 0.9615 to 0.9970 with an average value of 0.9836. The range for the Temkin isotherm (Figs. 12–14) was 0.9546–0.985 with an average value of 0.9797. While the R^2 for the Dubinin–Radushkevich isotherm (Table 2) in the range of 0.9744–0.9991, with an average value of 0.9997 (Table 3). The correlation coefficient of regression is used to determine the fitness of a model in describing the adsorption process. Based on this, these models are good indicators of the practical application of the synthesized cellulose nanomaterials for Cd(II) adsorption in aqueous solution. The order of the fitting was D-R > Langmuir > Freundlich > Temkin.

3.6. Adsorption thermodynamics

The thermodynamic parameters (ΔG , ΔS and ΔH) computed from the plots of $\ln K_c$ vs. $1/T$ for the adsorption of Cd(II) by aze2, aze10 and aze-TDI samples were calculated according to Milonjic [42] and are presented in Table 4. Data in the table show that the change in enthalpy (ΔH) of the adsorption of Cd(II) on aze-TDI, aze2 and aze10 has negative values, implying that the adsorption of Cd(II) was exothermic in nature, and based on the literature reports, positive values of ΔH , indicate that the physical adsorption mechanism contributed to the adsorption of Cd(II). The positive values of ΔS , indicate that a randomness increase at the solid–liquid interface during the adsorption of Cd(II) [40,41,45]. The negative values of ΔG implied that the adsorption process was spontaneous similar to the findings by Azeh et al. [8] and also by Milonjic [42] on saltbush biomass.

Table 2
Dubinin–Radushkevich (D-R) coefficients obtained from kinetic data

Metal ion	Azeh2			Azeh10			Azeh-TDI		
	q_s (mg/g)	$-B$ ($\text{mol}^2/\text{Jol}^2$)	E (kJ/mol)	q_s (mg/g)	$-B$ ($\text{mol}^2/\text{Jol}^2$)	E (kJ/mol)	q_s (mg/g)	$-B$ ($\text{mol}^2/\text{Jol}^2$)	E (kJ/mol)
Cd	0.2765	0.0017	17.15	0.2215	0.0014	18.89	0.3577	0.0038	11.47
				R^2	R^2	R^2	χ^2	χ^2	χ^2
				0.9744	0.044	0.2215	0.9912	0.024	0.9991
									0.1019

Table 3
Comparison of correlation coefficients for the sorption of Cd(II) ions

Model	Adsorbents		Average (R^2)
	Azeh2	Azeh-TDI	
Langmuir coefficients	R^2	R^2	0.9867
Freundlich coefficients	0.972	0.989	0.9836
Temkin coefficients	0.9615	0.9923	0.9883
Dubinin–Radushkevich (D-R)	0.9861	0.9985	0.9997
	0.9744	0.9912	

The values of ΔG , decreased with rising solution temperature from 310 to 360 K, implying that the adsorption of Cd(II) was thermodynamically favoured and the sorption process will proceed spontaneously in the forward direction to form more products [8]. The opposite thermal natures of this kind has been reported for As(V) and As(III) adsorption on red mud mixed oxides [43]. Positive values of ΔS reflect the affinity of the adsorbent material for Cd(II) ions and suggests possible structural changes in the Cd(II) species and the adsorbent material [44].

3.7. Adsorption kinetics

Kinetic study of Cd(II) sorption on azeh2, azeh10 and azeh-TDI at 300 K and pH 4.0 are tested for kinetic modelling by linear regression plots. Four kinetic models (pseudo-second-order (Fig. 15), power function (Fig. 16), Elovich (Fig. 17) and intraparticle diffusion (Fig. 18) were used to fit the experimental data by linear regression plots as shown in Tables 5 and 6. The pseudo-second-order kinetic model described the adsorption data for Cd(II) ions sorption on samples azeh2, azeh10 and azeh-TDI best with good correlation coefficients in the range of 0.9975–0.9995. The plot of t/q_t vs. t of the experimental data showed good agreement with q_e calculated. The equilibrium rate constants for Cd(II) sorption increased accordingly; azeh2 > azeh10 > azeh-TDI. The pseudo-second-order kinetics showed that the rate limiting step is chemisorption similar to the findings by Azeh et al. [8] on the adsorption of Pb(II) on cellulose nanomaterials and the sorption of Hg on palm shell powder by Kushwaha et al. [45]. While the power function model fits the kinetic data better compared with the intraparticle diffusion model. The coefficient of regression ranged from 0.7842 < R^2 > 0.9387 and 0.602 < R^2 > 0.8099. The constant “ v ” for the power function was 0.0372–0.1897. The value of v , was less than 1, indicating that the power function described the time dependent of Cd(II) ions adsorption on the synthesized nanomaterials. This observation was similar to the findings by Adegoke et al. [10] on Cr(VI) adsorption on synthetic hematite nanoparticles. The Elovich equation showed good correlation coefficient in the range of 0.784–0.9341. The initial sorption rate of Cd(II) on the modified samples followed the order: azeh-TDI > azeh10 > azeh2.

3.8. Intraparticle diffusion model

In order to find the mechanism that best describes the sorption of Cd by the nanomaterials, the intraparticle diffusion model was used. The rate constant was calculated from the slope of the plot of the amount of sorbate adsorbed, q_t (mg g^{-1}) vs. $t^{(1/2)}$ (square root). It was calculated by using the intraparticle diffusion model (Fig. 17) as shown by the equation [38–40].

$$q_t = K_{id}t^{1/2} + I \tag{6}$$

K_{id} ($\text{mg g}^{-1} \text{min}^{-1/2}$) is a measure of diffusion coefficient. I = intraparticle diffusion constant, that is, intercept of the line (mg g^{-1}). The constant I is directly proportional to the boundary layer thickness.

Table 4
Thermodynamic parameters for the adsorption of Cd(II) onto azeh-TDI, azeh2 and azeh10 samples

Sample	Temperature (K)	Metal	ΔG (kJ/mol)	ΔS (kJ/mol)	ΔH (kJ/mol)
Azeh-TDI	310	Cd	-4.4147×10^4	26.744×10^3	-40.59826×10^6
	320		-4.4147×10^4	27.606×10^3	-41.90788×10^6
	330		-4.7224×10^4	28.469×10^3	-43.21750×10^6
	340		-4.8803×10^4	29.332×10^3	-44.52712×10^6
	350		-4.9136×10^4	30.195×10^3	-45.83675×10^6
	360		-4.8970×10^4	31.057×10^3	-47.14637×10^6
Azeh2	310	Cd	-9.9103×10^4	44.017×10^3	-39.17557×10^6
	320		-10.4756×10^4	45.437×10^3	-40.43930×10^6
	330		-10.4756×10^4	46.857×10^3	-41.70302×10^6
	340		-10.4756×10^4	48.277×10^3	-42.96675×10^6
	350		-10.4756×10^4	49.697×10^3	-44.23048×10^6
	360		-9.9103×10^4	51.116×10^3	-45.49421×10^6
Azeh10	310	Cd	-10.4756×10^4	20.931×10^3	-36.85596×10^6
	320		-10.4756×10^4	21.606×10^3	-38.04486×10^6
	330		-10.4756×10^4	22.282×10^3	-39.23377×10^6
	340		-10.4756×10^4	22.957×10^3	-40.42267×10^6
	350		-9.9103×10^4	23.632×10^3	-41.61157×10^6
	360		-10.4756×10^4	24.307×10^3	-42.80047×10^6

Table 5
Adsorption kinetics constants for Cd(II) adsorption

Sample	Pseudo-second order			Power function			Intraparticle diffusion			Elovich		
	K_2 (g/mg/min)	q_e (mg/g)	R^2	K_p	V	R^2	K_{id}	I (mg/g)	R^2	a	b	R^2
Azeh2	2.386×10^{-4}	232.56	0.9987	67.1	0.1897	0.8952	4.3317	108.4	0.7163	32.85	29.933	0.8845
Azeh10	4.089×10^{-4}	161.29	0.9995	88.6	0.0867	0.9387	1.5755	112.19	0.8099	79.522	11.694	0.9341
Azeh-TDI	6.675×10^{-4}	232.56	0.9975	178.6	0.0372	0.7842	1.044	199.91	0.602	175.17	8.0965	0.784

The uptake of Cd by the samples revealed a three-stage pattern similar to the adsorption of Pb by the samples in our earlier report [8]. This indicates that the uptake of metal ions was predominantly by film diffusion than it does for the intraparticle diffusion [38,39,46,47]. The third stage revealed a steady diffusion of sorbate ions into the pore volume as revealed by the adsorption of Pb [8]. This was indicative of the fact that the pore volume was exhausted. According to the study by Biyan et al. [48], adsorption controlled by the intraparticle model is due to the preferential adsorption of sorbate in the micropore of the adsorbent.

The intraparticle diffusion rate constant, K_{id} , values obtained from the slope of the straight-line portions of plot of q_t vs. $t^{1/2}$ for various adsorbents is shown in Table 5. The correlation coefficients (R^2) for the intraparticle diffusion model are between 0.602 and 0.8099 at 300 K. It was observed that intraparticle rate constant values (K_{id}) and (I), varied accordingly; $4.3317 > 1.5755 > 1.044$ ($\text{mg g}^{-1}\text{min}^{-1/2}$) for azeh2, azeh10 and azeh-TDI while $I = 199.91 > 112.19 > 108.4$ for azeh-TDI, azeh10 and azeh2. According to these results, sample Azeh2 is highly porous and the adsorbent with the least surface porosity but high value of I was recorded with azeh-TDI. According to the study by Liu et al. [47], increase

in the values of K_{id} and I relates to increase in thickness of boundary layer of the adsorbents. Internal mass transfer was thus favoured according to the findings by Liu et al. [47]. Large value of the intercept implies large contribution of surface adsorption at the initial adsorbate concentration.

Also, the diffusion coefficients for the intraparticle transport of Cd(II) within the pores of nanomaterial particles have been calculated by employing the following equation [38].

$$D_i = 0.03 \times \frac{r^2}{t_{1/2}} \quad (7)$$

where D_i is the diffusion coefficients with the unit cm^2/s ; $t_{1/2}$ is the time (s) for half adsorption of Cd(II) ions and r is the average radius of the adsorbent particle in cm. Assuming spherical geometry of the sorbents. The value of r (average radius) was calculated from the pore radius of the adsorbents as obtained from BET analysis (15.10, 15.10 and 15.30 Å) as 1.51×10^{-7} , 1.51×10^{-7} and 1.53×10^{-7} cm for azeh2, azeh-TDI and azeh10 respectively [8]. According to Karthikeyan et al. [49], film diffusion is rate-determining step if the value film diffusion coefficient (D_f) is in the range of 10^{-6} – 10^{-8} cm^2/s .

If pore diffusion was to be the rate limiting, the pore diffusion coefficient (D_p) should be in the range of 10^{-11} – 10^{-13} cm²/s.

The order of diffusion coefficients was 10^{-11} – 10^{-13} cm²/s, which indicates that pore diffusion, had significant influence in the rate determining step similar to the findings by Azeh et al. [8]. This agreed with the long time taken for the adsorption process to attain equilibrium as reported by Dutta et al. [50].

3.9. Deduction of (K_{id}) in terms of % sorption

The Weber and Morris equation was used to predict the intraparticle diffusion in terms of percentage sorption (Fig. 19) of sorbate in solution by the adsorbent according to [38] reports.

$$R = K_{id} (t)^a \tag{8}$$

A linearized form of the equation is given as:

$$\log R = \log K_{id} + a \log (t) \tag{9}$$

where R = percentage of sorbate adsorbed, t = contact time (min), a = gradient of linear plot. The value of a depicts the adsorption mechanism. K_{id} is the intraparticle rate constant (time⁻¹). It is taken as rate factor, that is, percentage of sorbate adsorbed per unit time (mg g⁻¹ min^{-1(1/2)}).

According to the report by Itodo et al. [38], high values of K_{id} are indicators of an enhanced rate of adsorption and improved bonding between sorbate and sorbent particles. The application of the model gave a goodness of fit plots with correlation coefficients (R^2) in the order; $0.8922 > 0.8677 > 0.7614$ for Cd ion (azeh10 > azeh2 > azeh-TDI) and a value of a which was less than unity in the range of 0.0378–0.2343 and the intraparticle diffusion rate constant, K_{id} , for each adsorbent was 59.79/azeh-TDI, 29.41/azeh10 and 19.07/azeh2, respectively.

The enhanced rate of adsorption was linked to improved bonding between sorbent and sorbate systems. The K_{id} value with estimation based on percentage uptake of Cd ions was far less related to that which was based on q_t and $t^{1/2}$ plots ($K_{id} = 4.3317 > 1.5755 > 1.044$ [mg g⁻¹ min^{-1(1/2)}] for azeh2, azeh10

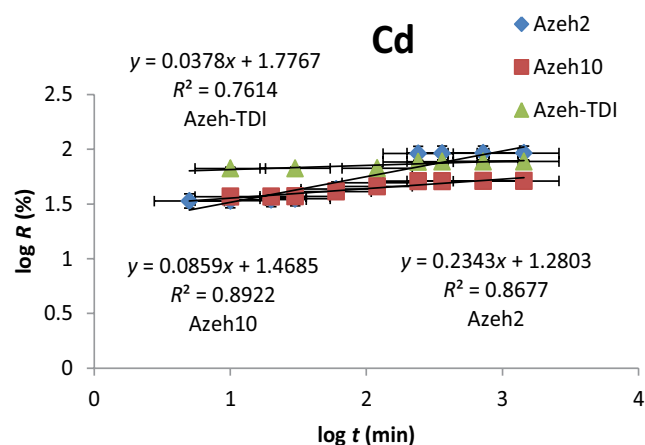


Fig. 19. log R vs. log t based on % uptake of Cd per unit time.

and azeh-TDI). This suggests that sorption mechanism is not intraparticle diffusion control, but a combination of mechanisms. However, irrespective of the linearity (high R^2 value) of the intraparticle diffusion plot, the sorption mechanism assumes intraparticle diffusion if the following conditions are satisfied:

- High R^2 values to ascertain applicability.
- Straight line which passes through the origin for the plot area q_t vs. $t^{1/2}$.
- Intercept $I < 0$.

According to the study by Azeh et al. [8] and Hameed [51], a validity test which deviates from (ii) and (iii) above shows that the mode of transport is affected by more than one adsorption mechanism.

3.10. Effect of ionic strength

The results of the effect of ionic strength are reported in this section. Increasing the ionic strength concentrations, caused a decrease in Cd(II) removal, which agreed with literature reports [10,52,53]. The amount removed (q_e) increased with decreasing ionic strength of the metal solutions as the contact time increased (Fig. 20). At the equilibrium point of contact (240 min), the maximum q_e was recorded for all the three point ionic strengths, 0.1, 0.3 and 0.5 mol dm⁻³ investigated. The results showed that at 0.1 mol dm⁻³, the nano-structured particles performed best. Similar observations have been reported by Adegoke et al. [10] and Lata et al. [54]. As shown in Fig. 21, the highest removal efficiency of 99.1%, occurred when the contact time was 60 min and the ionic strength was 0.1 mol dm⁻³ compared with 75.6% and 72.1% for the 0.3 and 0.5 mol dm⁻³ ionic strengths, respectively (Table 6). This could be explained by the fact that, at higher concentrations, the positively charged sodium ions effectively compete with the metal ions for the binding sites on the adsorbent surface, which can restrict the number of Cd(II) ions being adsorbed. This process generally caused a decrease in Cd(II) adsorption with increasing ionic strength

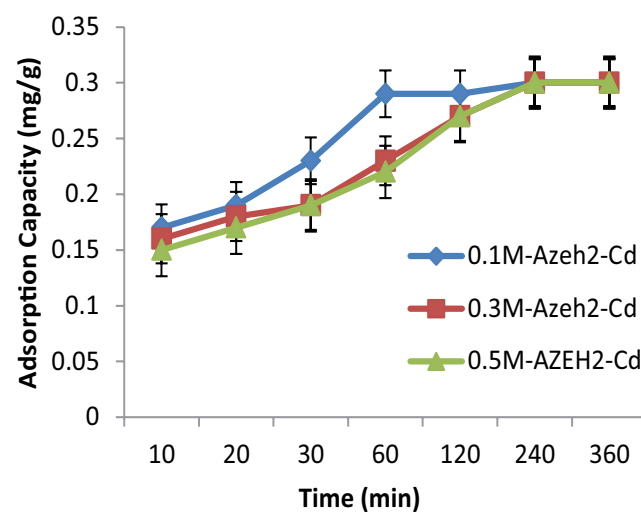


Fig. 20. Effect of ionic strength on Cd removal by azeh2.

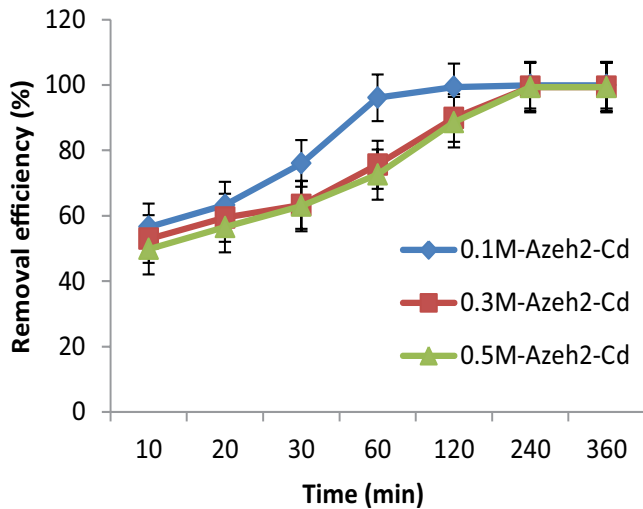


Fig. 21. Effect of ionic strength on removal efficiency of Cd adsorption by aze2.

of the aqueous solution. The adsorption capacity in this study decreased with increasing ionic strength, indicating that Cd(II) adsorption depend on the ionic strength of the solution.

3.11. Desorption studies

Fig. 22 shows the effects of different HNO_3 concentrations: 0.1, 0.2, 0.3 and 0.5 mol dm^{-3} on Cd(II)-loaded

cellulose nanoparticles against desorption contact time are shown. The use of acids exhibits similar desorption efficiency of metal ions from aze2-TDI and aze2 nanoparticles. Desorption efficiency increased with increasing acid concentration as a function of time which was similar to other literature reports [55–57]. A 100% desorption efficiency was attained using 0.5 mol dm^{-3} HNO_3 (Table 7). This implies that at this concentration, higher desorption efficiency can be achieved and it is also economical. This acid can be used as desorbing agent. This observation is likely attributable to the increase in acid concentration leading to the accumulation of H^+ in solution, thus increasing the concentration gradient of Cd(II) and H^+ and resulting in an increased driving force for ion exchange. This process favours the desorption process. The maximum desorption capacity of the cellulose nanoparticle type adsorbent aze2 and aze2-TDI reached 0.230 mg/g with desorption efficiency of 100% at 0.5 mol dm^{-3} HNO_3 . Under acidic conditions, protons are furnished on the surface of the sorbent which allows desorption of positively charged ions [58]. Therefore, 0.5 mol dm^{-3} was the best eluent. Acid solutions were used in the concentration range 0.1–0.5 mol dm^{-3} since higher concentrations could damage the structure of the sorbent. The results showed that both adsorbents are easier to regenerate. Nitric acid has been used as an eluent for the stripping of lead from algal biomass [54]. A 100% recovery of Cu^{2+} adsorbed on spherical cellulose using 2.4 mol/L of HCl has been reported [55]. A satisfactory recovery rate of 75%–100% was achieved for all the nanoparticle adsorbents in the concentration range 0.1–0.5 mol dm^{-3} (Table 7). The study showed that HNO_3 was sufficiently useful for

Table 6
Effect of ionic strength on Cd(II) removal ($C_i = 3$ mg/L)

Time (min)	0.1 M		0.3 M		0.5 M	
	Q_e (mg/g)	RE (%)	Q_e (mg/g)	RE (%)	Q_e (mg/g)	RE (%)
10	0.17	56.6	0.16	52.9	0.15	49.83
20	0.19	63.3	0.18	59.4	0.17	56.50
30	0.23	76.0	0.19	63.3	0.19	63.0
60	0.29	96.1	0.23	75.6	0.22	72.6
120	0.29	99.4	0.27	89.9	0.27	88.6
240	0.30	99.9	0.29	99.4	0.30	99.3
360	0.30	99.9	0.30	99.4	0.30	99.3

Table 7
Desorption of Cd(II) from aze2-Cd loaded $C_e = 0.23$ mg/g

Time (min)	0.1 M		0.2 M		0.3 M		0.5 M	
	C_t	RE (%)						
10	0.001	0.44	0.001	0.44	0.002	0.87	0.003	1.3
20	0.002	0.87	0.006	2.61	0.009	3.9	0.008	3.5
30	0.012	5.22	0.018	7.83	0.017	7.4	0.019	8.3
60	0.028	12.2	0.042	18.26	0.043	18.7	0.051	22.2
120	0.031	13.5	0.086	37.4	0.098	42.6	0.106	46.1
240	0.218	94.8	0.192	83.47	0.106	46.1	0.230	100

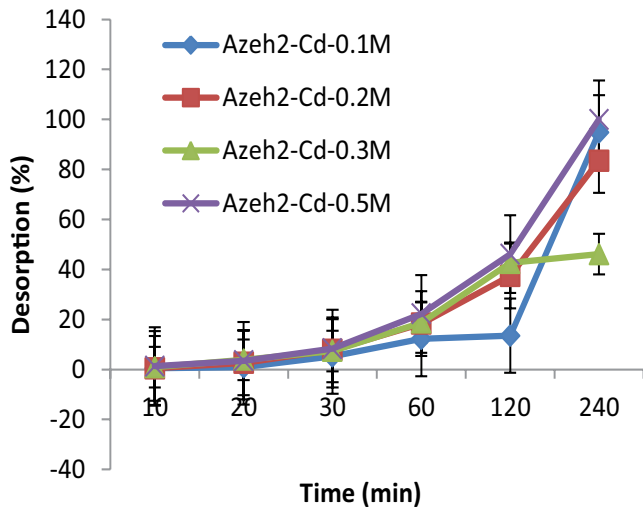


Fig. 22. Desorption efficiency of Cd-azeh2-loaded nanoparticle.

desorption of the metal ions from adsorbents. This also means that the adsorbents could be reused in order to remove heavy metals from aqueous solutions. Desorption of Cd from the nanoparticle adsorbents showed different trends. In Table 7, one could see that the desorption process of Cd(II) ions from azeh2-Cd-loaded cellulose nanoparticles was slow. At the equilibrium time of 240 min, 46%–100% desorption was achieved in the concentration range 0.1–0.5 mol dm⁻³ HNO₃. The slow desorption processes implied that Cd(II) ions are tightly bound to the adsorbents surface. This further supports the mechanism of sorption as predicted by the intraparticle diffusion kinetics and Langmuir model, which revealed that chemisorption partly contributes to the sorption mechanisms.

3.12. Desorption kinetics of Cd(II)

Figs. 23–26 presented desorption kinetics performance of the azeh2-Cd-loaded cellulose nanoparticles. A satisfactory desorption rate of 75%–100% desorption efficiency was achieved within the equilibrium time 240 min., indicating a slow desorption kinetics. This implied that chemisorption contributed to the adsorption process. Three kinetic

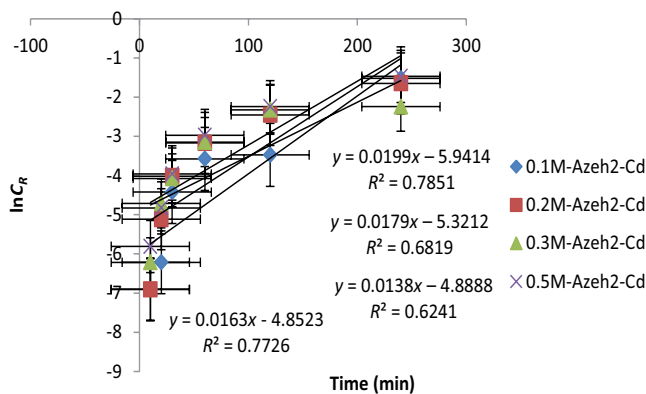


Fig. 23. First order desorption kinetics azeh2-Cd.

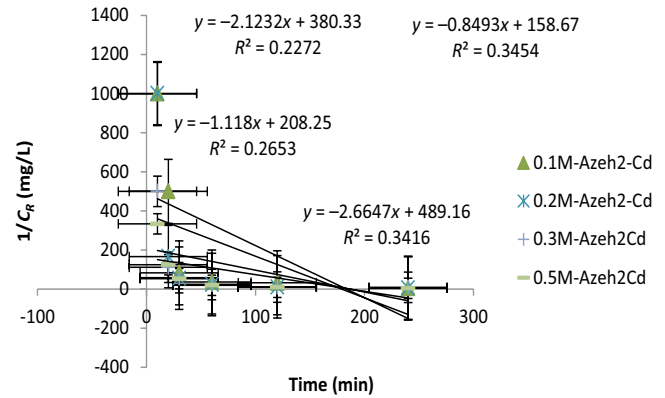


Fig. 24. Second order desorption kinetics azeh2-Cd.

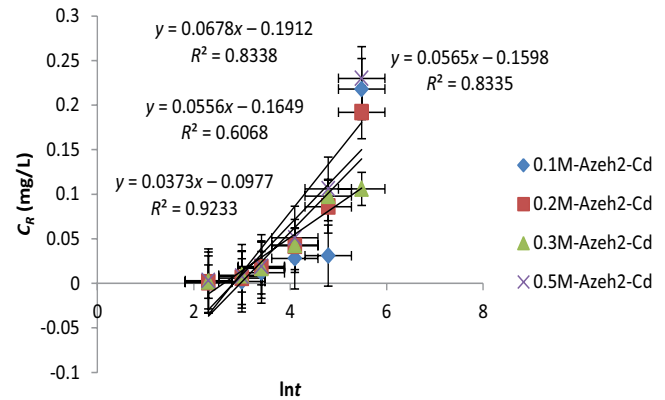


Fig. 25. Elovich desorption kinetics azeh2-Cd.

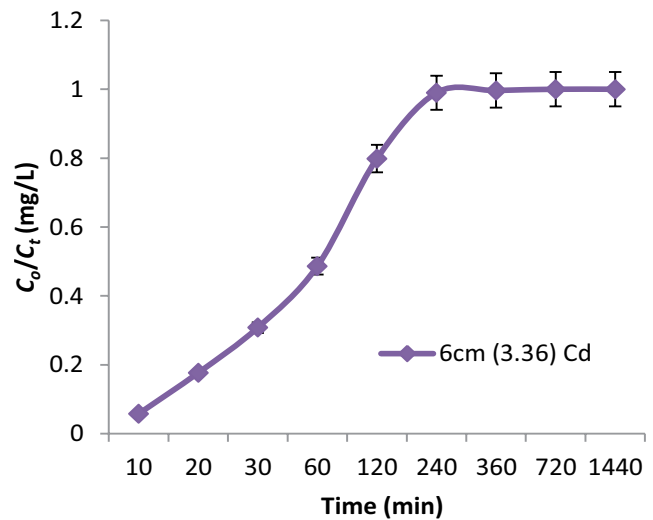


Fig. 26. Breakthrough curve for bed depth, 6 cm (3.36 g) Cd and flow rate, 4 mL/min.

models, namely, first order model, second order and the Elovich model were applied to fit the desorption data of Cd(II) desorption kinetics from the cellulose nanoparticles azeh2-Cd. The kinetic models and their model parameters are shown in Table 8. The correlation coefficient (R^2) and kinetic

Table 8

Correlation coefficient (R^2) and kinetic constants of the applied desorption kinetics models for the desorption kinetics of azeh2-Cd-loaded cellulose nanoparticles at different molar concentrations

Sample	1st order kinetic model			2nd order kinetic model			Elovich model		
	K_{R1} (min ⁻¹)	$\ln C_{RF}$	R^2	K_{R2} (g mg ⁻¹ min ⁻¹)	$1/C_{RF}$ (mg L ⁻¹)	R^2	β (g mg ⁻¹)	a (g mg ⁻¹ min ⁻¹)	R^2
Azeh2-Cd/0.1 M	0.0199	1.782	0.7851	-2.665	0.0024	0.3416	17.99	-5.39	0.6068
Azeh2-Cd/0.2 M	0.0179	1.671	0.6819	-2.123	0.0026	0.2272	17.69	-5.40	0.8335
Azeh2-Cd/0.3 M	0.0138	1.587	0.6241	-1.118	0.0048	0.2653	26.81	-6.31	0.9233
Azeh2-Cd/0.5 M	0.0163	1.579	0.7726	-0.849	0.0067	0.3454	14.75	-5.04	0.8338
Average (R^2)			0.7159			0.2949			0.7994

rate constants of the three models are shown in Table 9. The results indicated that the cellulose nanoparticles, azeh2-Cd studied, the Elovich model showed the best fitting (R^2) for the metal-loaded cellulose nanoparticles. The order of fitting was Elovich > first order > second order. Elovich was reported to show the best correlation coefficient for copper ion-loaded P-Polyamines desorption kinetics [59]. In addition, the desorption efficiency against time for azeh2-Cd-loaded cellulose nanoparticles complied with the Elovich kinetic model parameters (β and α) as shown in Table 8. Chien and Clayton [60] pointed out that a decrease in the value of β and/or an increase of α , indicates the increase of the reaction rate. They also showed that the parameter β , rather than α , would be a useful indicator for the comparison of the reaction rate. The results in this study followed the Chien and Clayton's [60] conclusions.

3.13. Column adsorption

3.13.1. Adsorption of Cd from industrial effluent

Table 10 reveals that as the column adsorption of Cd(II) proceeds, the adsorption capacity increases while the removal efficiency decreases. This was attributed to the fact that as the influent stream pass through the packed bed, more solute molecules are trapped and retained by the nanocellulose adsorbent and as the process continued, it leads to increase in the adsorption capacity until saturation of the bed. As this process continued with time, the amount of solute captured and retained from the flow stream by the adsorbent decreased, resulting in an increase in the amount of solute concentration in the effluent stream. Hence, the removal efficiency of the adsorbent decreased. It could be seen in Table 10 that for 270 and 1,440 min, the adsorption capacities were 1.370 and 2.740 mg/g while the removal

Table 9

Model parameters of the Elovich model applied to the azeh2-Cd(II)-loaded cellulose nanoparticle desorption kinetics

Sample	Azeh2-Cd			
	0.1	0.2	0.3	0.5
Molar concentration (mol dm ⁻³)				
β (L mmol ⁻¹)	17.99	17.69	26.81	14.75
α (L mg ⁻¹ S ⁻¹)	-5.39	-5.40	-6.31	-5.04

efficiency for these two elution times were 0.00 mg/g. The adsorption capacities of the column mode study are higher than that of batch study. Tables 10 and 11 also show that at breakthrough point of 0.9 (Figs. 26–29), the bed adsorption capacity was 2.740 mg/g of Cd, and 2.301 mg/g for the bed depth of 6 and 8 cm, respectively. The amount of Cd removed was linked to the initial metal ion concentration in the effluent [58–61].

3.13.2. Effect of bed depth

It was observed in Fig. 28 that at the same breakthrough point, the breakthrough time increased with decrease in

Table 10

Breakthrough curve for $Z = 6$ cm, $f = 4$ mL/min, $g = 3.36$ g, $C_0 = 1.598$ mg/L Cd

Time (min)	C_t (mg/g)	q_B (mg/g)	C_t/C_0	RE (%)
10	0.099	0.019	0.058	94.24
20	1.079	0.038	0.177	82.35
30	3.701	0.057	0.308	69.21
60	7.041	0.114	0.486	51.37
120	10.481	0.228	0.799	20.15
240	15.694	0.457	0.989	0.75
360	18.091	0.685	0.996	0.37
720	18.101	1.370	1.000	0
1,440	18.102	2.740	1.000	0

Table 11

Breakthrough curve data for $Z = 8$ cm, $f = 4$ mL/min, $g = 4$ g, $C_0 = 1.598$ mg/L Cd

Time (min)	C_t (mg/g)	q_B (mg/g)	C_t/C_0	RE (%)
10	0.19	0.016	0.119	88.11
20	0.534	0.032	0.334	66.58
30	0.787	0.048	0.493	50.75
60	1.367	0.096	0.855	14.45
120	1.564	0.192	0.979	2.13
240	1.59	0.384	0.995	0.50
360	1.598	0.575	1.000	0
720	1.598	1.151	1.000	0
1,440	1.598	2.301	1.000	0

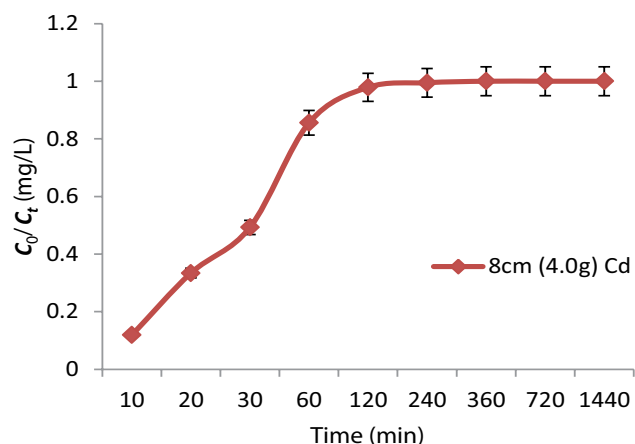


Fig. 27. Breakthrough curve for bed depth, 8 cm (4 g) Cd and flow rate, 4 mL/min.

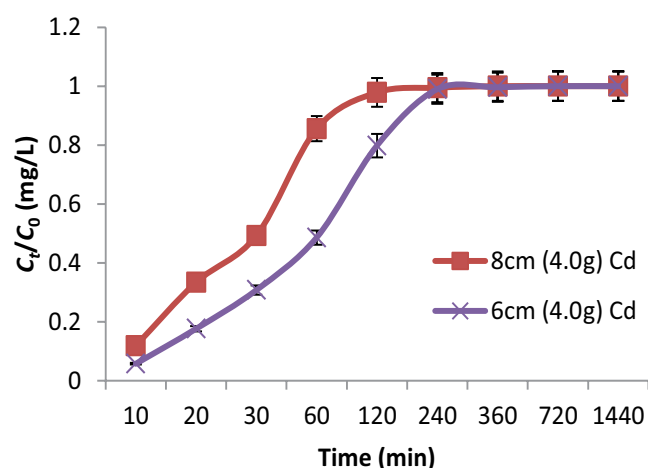


Fig. 28. Breakthrough curve for different bed depths for Cd.

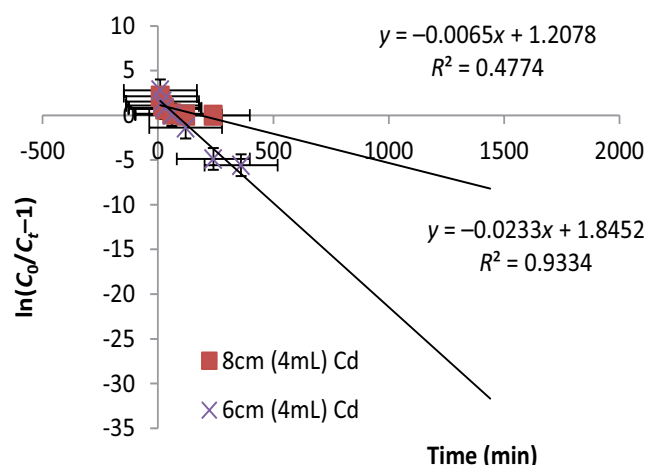


Fig. 29. Thomas kinetic plot for the adsorption of Cd in a binary.

bed depth. This observation agreed with the results of the effect of adsorbent dose on Cd(II) adsorption. Small column depth of the nanocellulose particle showed high adsorption capacity and removal efficiency due to increased surface

area and availability of more binding sites for sorption on the nanoparticles. It was also observed that at any breakthrough point, the corresponding breakthrough time, the capacity and the volume of effluent treated increased with decreasing bed depth. This implied that the equilibrium sorption capacity decreased with increasing bed height, implying that at smaller bed height, the adsorbate concentration ratio increased more rapidly than for a higher bed height. Furthermore, the bed is saturated in less time for smaller bed heights as small bed height corresponds to less amount of adsorbent. This means that as the bed depth was increased, the adsorbent mass also increased while its performance decreased. This observation was in agreement with the literature report on palm fibre [62]. However, this contradicts the results of the study on activated carbon by Bohli et al. [36], likewise, the study on rubber wood dust [58], and on lignocellulosic waste [63]. Tables 12 and 13 and Fig. 28 show the breakthrough characteristics with respect to increase in bed depth. The breakthrough curve shows that with small bed depth, an extended breakthrough time was observed. The tables showed that the longer the breakthrough time, the higher the breakthrough capacity of the column and this agreed with the study by Mohammad [40], and Swarup and Umesh [58]. It was observed that the breakthrough time was not reached as quickly compared with other literature reports [63]. This means that larger volumes of effluent could be treated with small quantity of the nanocellulose adsorbent before the column is completely exhausted. This is economical for industrial applications. This was as a result of the slower transport of the metal ions in the effluent onto the surface of the adsorbent as a consequence of diffusion mechanism.

3.14. Dynamic adsorption models

3.14.1. Thomas model

The adsorption data were fitted to three well-established fixed-bed adsorption models namely, Adam–Bohart, Thomas and Yoon–Nelson models. The kinetic coefficient K_T and the adsorption capacity of the bed, q_0 were determined from the plot of $\ln(C_0/C_t - 1)$ against time (t). Thomas model parameters were obtained from the slope and intercept of Fig. 29 and are presented in Table 14. The table showed that the theoretical breakthrough capacity (q_0) for Cd(II) removed increased with increasing bed depth of the column. This observation has been reported in literature [40,61–63]. The results of this study are similar to the findings by Rahman and Khan [64] on the adsorption of nitrate using poly-*o*-toluidine zirconium (IV) ethylenediamine as adsorbent packed in a fixed-bed column. It is seen that q_0 is concentration dependent of the effluent as reported in literature [62]. This was due to low number of metal ions for the adsorption sites on the surface of the nanoparticles. The determined coefficients and relative constants were obtained using linear regression analysis. It was observed that K_{TH} values for Cd(II) removed decreased with increase in the column depth. The R^2 values were 0.93 and 0.47 for Cd(II) removed for the bed depths of 6 and 8 cm, respectively. This indicates that the column experimental data for the 6 cm bed depth fitted well to the Thomas model, which implies that it can be used to describe the column performance on the adsorption of Cd(II) from industrial effluent.

Table 12
Breakthrough characteristics of Cd, 3.36 g

Breakthrough points		0.05			0.3			0.9		
Z (cm)	f (mL)	t _B (min)	V _{eff} (L)	q _B (mg/g)	t _B (min)	V _{eff} (L)	q _B (mg/g)	t _B (min)	V _{eff} (L)	q _B (mg/g)
6	4	20	80	0.431	60	240	1.293	720	2,880	15.516
6	4	10	40	0.019	30	120	0.543	360	1,440	6.517

Table 13
Breakthrough characteristics of Cd, 4 g

Breakthrough points		0.1			0.3			0.8			0.9		
Z (cm)	f (mL)	t _B (min)	V _{eff} (L)	q _B (mg/g)	t _B (min)	V _{eff} (L)	q _B (mg/g)	t _B (min)	V _{eff} (L)	q _B (mg/g)	t _B (min)	V _{eff} (L)	q _B (mg/g)
8	4	20	80	0.362	30	120	0.543	120	480	2.172	360	1,440	6.517
8	4	10	40	0.016	20	80	0.032	60	240	0.096	120	480	0.192

Table 14
Thomas model parameters

Z (cm)/metal ion	f (mL/min)	K _{TH}	q ₀ (mg/g)	R ²
6/Cd	4	0.01458	0.192	0.9334
8/Cd	4	0.00407	0.297	0.4774

Table 15
Yoon–Nelson model parameters

Z (cm)/metal ion	f (mL/min)	K _{YN}	τ (min)	R ²
6/Cd	4	0.0233	79.19	0.9334
8/Cd	4	0.0297	33.67	0.8707

3.14.2. Yoon–Nelson model

The values of K_{YN} and τ are listed in Table 15. Yoon–Nelson model parameters were obtained from the slope and intercept of Fig. 30. A plot of ln(C_t/C₀ - C_t) vs. t gives a straight line with slope of K_{YN} and intercept of -τ × K_{YN}. From Table 15, the rate constant K_{YN} decreased with increased bed depth and the 50% breakthrough time τ increased with increase in effluent initial concentration and this agrees with literature findings [40,52]. The 50% breakthrough time (τ), decreased with increase in bed depth [55]. The increase in τ could also be attributed to the initial concentration of the effluent. Generally, R² values are regarded as implying high practical applicability of the adsorbent, and as such the R² values obtained (0.93 and 0.87) indicates that the Yoon–Nelson model can be used to describe the behaviour of the adsorption of Cd(II) in a binary metal system in a fixed-bed column adsorption.

3.14.3. Adam–Borhart model

Adam–Borhart model parameters were obtained from the slope and intercept of the plot of C_t/C₀ against time (Fig. 31). From Table 16, it was observed that the values of N₀ decreased with increase in bed depth for Cd(II) removal, which was due to initial metal ion concentration in the effluent [39,60], the values of K_{AB} increased with increase in bed depth [58–61]. Although the Adam–Borhart model provides a simple and comprehensive approach to evaluate adsorption-column test, its validity is limited to the range of conditions used. The low value of coefficient

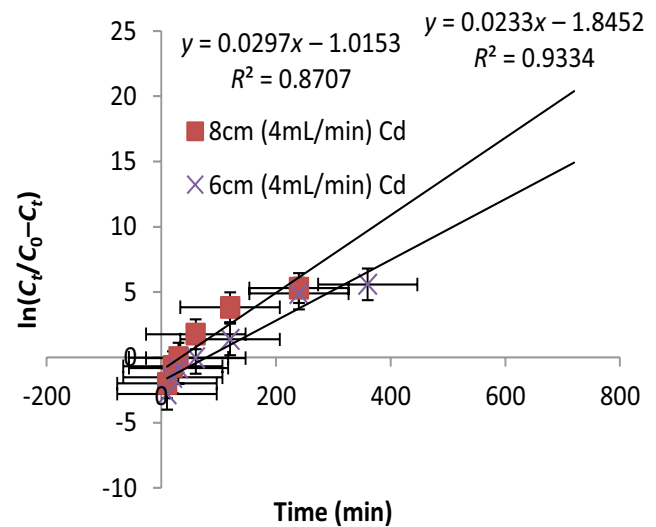


Fig. 30. Yoon–Nelson kinetic plot for the adsorption of Cd.

Table 16
Adam–Borhart model parameters

C ₀ (mg/L)	Z (cm)/metal ion	f (mL/min)	K _{AB} (L/g min)	N ₀ (mg/l)	R ²
1.598	6/Cd	4	0.00375	299	0.5725
1.598	8/Cd	4	0.00408	148	0.4774

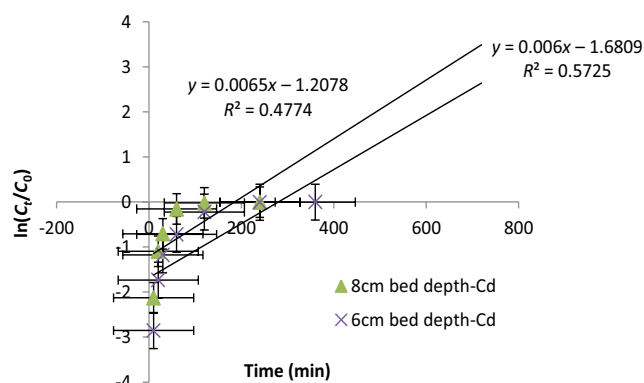


Fig. 31. Breakthrough curve by Adam–Borhart model at different bed height.

of determination R^2 (0.57 and 0.47) as observed in Table 16 shows that the experimental data did not fit well to the model.

4. Conclusion

The adsorption kinetics of Cd^{+2} ions onto aze2, aze10 and aze-TDI samples followed a pseudo-second-order kinetics. The intraparticle diffusion coefficients ranged from 1×10^{-11} to $7 \times 10^{-13} \text{ cm}^2/\text{s}$, which showed the contribution from pore diffusion controlled mechanism. Deduction from K_{id} in terms of % sorption showed that sorption mechanism of Cd^{+2} was a combination of mechanisms. The Langmuir, Freundlich, Temkin and D-R models were used to describe the adsorption process of the adsorbate. The negative ΔG and ΔH indicated that the adsorption of $\text{Cd}(\text{II})$ by aze2, aze10 and aze-TDI was exothermic, feasible and spontaneous in nature. The positive ΔS indicates the increase in randomness of the system. In this study, the synthesized nanoparticles showed high adsorption capacities and removal efficiency for Cd^{+2} ions in aqueous solution at pH 4. Pore diffusion had significant influence in the rate determining step of the adsorption of Cd^{+2} ions. Treatment of industrial effluent using fixed-bed column adsorption showed that small bed depth had best performance. Column adsorption capacities were higher than the values obtained in batch mode study. R^2 values showed that Thomas and Yoon–Nelson models could be used to describe the behaviour of the column for the adsorption of $\text{Cd}(\text{II})$. The microbial load of the effluent was determined before and after it has passed through the column. The initial bacteria colony count due to microbiological contaminants in the effluent was 2,000 cfu/mL, which was reduced to 30 cfu/mL after 1,440 min of treatment in the column. This value was, however, lower than the acceptable limit of 1×10^2 cfu/mL set by the World Health Organization (WHO). The study concluded that the nanocelluloses have the potentials for applications in water clean-up processes.

References

- [1] S. Sato, K. Yoshihara, K. Moriyama, M. Machida, H. Tatsumoto, Influence of activated carbon surface acidity on adsorption of heavy metal ions and aromatics from aqueous solution, *Appl. Surf. Sci.*, 253 (2007) 8554–8559.
- [2] X. Li, Y. Tang, Z. Xuan, Y. Liu, F. Luo, Study on the preparation of orange peel cellulose adsorbents and biosorption of Cd^{2+} from aqueous solution, *Sep. Purif. Technol.*, 55 (2007) 69–75.
- [3] D.W. O’Connell, C. Birkinshaw, T.F. O’Dwyer, Heavy metal adsorbents prepared from the modification of cellulose: a review, *Bioresour. Technol.*, 99 (2008) 6709–6724.
- [4] M.A. Barakat, New trends in removing heavy metals from industrial wastewater, *Arabian J. Chem.*, 4 (2011) 361–377.
- [5] D. Sud, G. Mahajan, M.P. Kaur, Agricultural waste material as potential adsorbent for sequestering heavy metal ions from aqueous solutions – a review, *Bioresour. Technol.*, 99 (2008) 6017–6027.
- [6] F. Fu, Q. Wang, Removal of heavy metal ions from wastewaters: a review, *J. Environ. Manage.*, 92 (2011) 407–418.
- [7] G.B. Adebayo, N. Abdus-salam, S.A. Elelu, Adsorption of lead (II) ions by activated carbon prepared from different parts of *jatropha curcas* plant, *Ilorin J. Sci.*, 1 (2014) 28–49.
- [8] Y. Azeh, G.A. Olatunji, F.A. Adekola, Modified/unmodified nanoparticle adsorbents of cellulose origin with high adsorptive potential for removal of $\text{Pb}(\text{II})$ from aqueous solution, *Eur. Sci. J.*, 13 (2017) 425–458.
- [9] M. Ahmad, S. Ahmed, B.L. Swami, S. Ikram, Adsorption of heavy metal ions: role of chitosan and cellulose for water treatment. *IJP*, 2 (2015) 280–289.
- [10] H.I. Adegoke, F.A. Adekola, O.S. Fatoki, B.J. Ximba, Adsorption of $\text{Cr}(\text{VI})$ on synthetic hematite ($\alpha\text{-Fe}_2\text{O}_3$) nanoparticles of different morphologies, *Korean J. Chem. Eng.*, 31 (2014) 142–154.
- [11] J.A. Shatkin, T.H. Wegner, E.M.T. Bilek, J. Cowie, Market projections of cellulose nanomaterial-enabled products - Part 1: applications, *Tappi J.*, 13 (2014) 1–8.
- [12] M.E. Argun, Ş. Dursun, Removal of heavy metal ions using chemically modified adsorbents, *J. Int. Environ. Appl. Sci.*, 1 (2006) 27–40.
- [13] O.K. Junior, L.V.A. Gurgel, R.P. de Freitas, L.F. Gil, Adsorption of $\text{Cu}(\text{II})$, $\text{Cd}(\text{II})$, and $\text{Pb}(\text{II})$ from aqueous single metal solutions by mercerized cellulose and mercerized sugarcane bagasse chemically modified with edta dianhydride (EDTAD), *Carbohydr. Polym.*, 77 (2009) 643–650.
- [14] N. Rahman, M. Nasir, Application of Box–Behnken design and desirability function in the optimization of $\text{Cd}(\text{II})$ removal from aqueous solution using poly(o-phenylenediamine)/hydrous zirconium oxide composite: equilibrium modeling, kinetic and thermodynamic studies, *Environ. Sci. Pollut. Res.*, 25 (2018) 26114–26134.
- [15] D.W. O’Connell, C. Birkinshaw, T.F. O’Dwyer, Design of a novel cellulose-based adsorbent for use in heavy metal recovery from aqueous waste streams, *Water Pollut. VIII Modell. Monit. Manage.*, 95 (2006) 1–10.
- [16] H.H. Abdel-Razik, A.M. El-Asmar, M. Abbo, Heavy metal adsorbents based on chelating amidoximated grafted cellulose, *Int. J. Basic Appl. Chem. Sci.*, 3 (2013) 1–9.
- [17] Z. Liu, H. Wang, C. Liu, Y. Jiang, G. Yu, X. Mu, X. Wang, Magnetic cellulose-chitosan hydrogels prepared from ionic liquids as reusable adsorbent for removal of heavy metal ions, *Chem. Commun.*, 48 (2012) 7350–7352.
- [18] L. Xia, Z. Huang, L. Zhong, F. Xie, C.Y. Tang, C.P. Tsui, Bagasse cellulose grafted with an amino-terminated hyper-branched polymer for the removal of $\text{Cr}(\text{VI})$ from aqueous solution, *Polymers*, 10 (2018) 1–15.
- [19] I. Filpponen, The Synthetic Strategies for Unique Properties in Cellulose Nanocrystals Materials, Dissertation, Graduate Faculty of North Carolina State, Raleigh, North Carolina 2009.
- [20] M.F. Rosa, E.S. Medeiros, J.A. Malmonge, K.S. Gregorski, D.F. Wood, L.H.C. Mattoso, G. Glenn, W.J. Orts, S. H. Imam, Cellulose nanowhiskers from coconut husk fibers: effect of preparation conditions on their thermal and morphological behaviour, *Carbohydr. Polym.*, 81 (2010) 83–92.
- [21] Y. Azeh, G.A. Olatunji, F.A. Adekola, Synthesis and characterization of cellulose nanoparticles and its derivatives using a combination of spectro-analytical techniques, *Int. J. Nano. Med. Eng.*, 2 (2017) 65–94.
- [22] E. Samuel, T. Wim, Surface modification of cellulose nanocrystals, *Nanoscale*, 6 (2014) 7764–7779.

- [23] B.G.N. Sewwandi, M. Vithanage, N.I.M. Mojuod, K. Kawamoto, S. Hamamoto, Removal of Heavy Metals from Wastewater Using Agricultural Waste Materials, EE2 Seminar, Water and Environment in Asia's Developing Communities, 1st July, 2012.
- [24] P. Liu, Adsorption Behaviour of Heavy Metal Ions from Aqueous Medium on Nanocellulose, PhD Thesis, Division of Material Science Department of Engineering Sciences and Mathematics Lulea University of Technology Lulea, Sweden, 2015.
- [25] Y.H. Lim, I.M.L. Chew, T.S.Y. Choong, M.C. Tan, K.W. Tan, Nanocrystalline cellulose isolated from oil palm empty fruit bunch and its potential in cadmium metal removal, MATEC Web of Conferences, 59 (2016) 5, doi.org/10.1051/mateconf/20165904002.
- [26] N.D. Thanh, H.L. Nhung, Cellulose Modified with Citric Acid and Its Absorption of Pb²⁺ and Cd²⁺ Ions, 3rd International Electronic Conference on Synthetic Organic Chemistry (ECSOC-13), 1–30 November, 2009, pp. 1–13.
- [27] S. Hokkanen, E. Repo, T. Suopajarvi, H. Liimatainen, J. Niinimaa, M. Sillanpää, Adsorption of Ni(II), Cu(II) and Cd(II) from aqueous solutions by amino modified nanostructured microfibrillated cellulose, Cellulose, 21 (2014) 1471–1487.
- [28] T. Suopajarvi, Functionalized Nanocellulose in Wastewater Treatment Applications, Dissertation to be Presented, Linnamäe, University of Oulu, Oulu, 2015.
- [29] S.N.M. Yusoff, A. Kamari, W.P. Putra, C.F. Ishak, A. Mohamed, N. Hashim, I.M.D. Isa, Removal of Cu(II), Pb(II) and Zn(II) ions from aqueous solutions using selected agricultural wastes: adsorption and characterisation studies, J. Environ. Prot., 5 (2014) 289–300.
- [30] Z. Hubicki, D. Kołodyńska, Selective Removal of Heavy Metal Ions from Waters and Waste Waters Using Ion Exchange Methods, Intech, 2012, pp. 193–240.
- [31] M.A. Hubbe, S.H. Hasan, J.J. Ducoste, Cellulosic substrates for removal of pollutants from aqueous systems: a review 1 Metals, Bioresour., 6 (2011) 2161–2287.
- [32] A.K. Asiagwu, Sorption kinetics of Pb(II) and Cd(II) ions via biomass surface of plantain peel waste, Ijrras, 13 (2012) 626–635.
- [33] X. Zhang, S. Zeng, S. Chen, Y. Ma, Change of the extractability of Cadmium added to different soils: aging effect and modeling, Sustainability, 10 (2018) 1–14.
- [34] N. Abdus-Salam, F.A. Adekola, The influence of pH and adsorbent concentration on adsorption of lead and zinc on a natural goethite, Afr. J. Sci. Technol., 6 (2005) 55–66.
- [35] A. Mautner, H.A. Maples, T. Kobkeathawin, V. Kokol, Z. Karim, K. Li, A. Bismarck, Phosphorylated nanocellulose papers for copper adsorption from aqueous solutions, Int. J. Environ. Sci. Technol., 13 (2016) 1861–1872, doi. 10.1007/s13762-016-1026-z.
- [36] T. Bohli, I. Villaescusa, A. Ouederni, Comparative study of bivalent cationic metals adsorption Pb(II), Cd(II), Ni(II) and Cu(II) on olive stones chemically activated carbon, J. Chem. Eng. Process Technol., 4 (2013) 1000158.
- [37] L.V.A. Gurgel, L.F. Gil, Adsorption of Cu(II), Cd(II), and Pb(II) from aqueous single metal solutions by succinylated mercerized cellulose modified with triethylenetetramine, Carbohydr. Polym., 77 (2009) 142–149.
- [38] A.U. Itodo, F.W. Abdulrahman, L.G. Hassan, S.A. Maigandi, H.U. Itodo, Intraparticle diffusion and intraparticle diffusivities of herbicide on derived activated carbon, Research., 2 (2010) 74–86.
- [39] S.M. Yakout, E. Elsherif, Batch kinetics, isotherm and thermodynamic studies of adsorption of strontium from aqueous solutions onto low cost rice-straw based carbons, Carbon Sci. Technol., 1 (2010) 144–153.
- [40] Y.S. Mohammad, Performance Evaluation of Treated Rice Husk Activated Carbon in Water Treatment and Removal of Phenol, PhD Thesis, Ahmadu Bello University Zaria, Nigeria, 2015.
- [41] S. Goswami, U.C. Ghosh, Studies on adsorption behaviour of Cr(VI) onto synthetic hydrous stannic oxide, Water SA, 31 (2005) 597–602.
- [42] S.K. Milonjic, A consideration of the correct calculation of thermodynamic parameters of adsorption, J. Serb. Chem. Soc., 72 (2007) 1363–1367.
- [43] S. Sadaf, H.N. Bhatti, S. Ali, K. Rehman, Removal of indosol turquoise FBL dye from aqueous solution by bagasse, a low cost agricultural waste: batch and column study, Desal. Wat. Treat., 52 (2014) 184–198.
- [44] L. Zeng, Arsenic adsorption from aqueous solutions on an Fe(III)-Si binary oxide adsorbent, Water Qual. Res. J. Can., 39 (2004) 267–275.
- [45] S. Kushwaha, S. Sodaye, P. Padmaja, Equilibrium, kinetics and thermodynamic studies for adsorption of Hg (II) on palm shell powder, World Acad. Sci. Eng. Technol., 19 (2008) 597–603.
- [46] Y.S. Ho, J.C.Y. Ng, G. McKay, Kinetics of pollutant sorption by biosorbents: review, Sep. Purif. Methods, 29 (2000) 189–232.
- [47] L. Liu, J. Liu, H. Li, H. Zhang, J. Liu, H. Zhang, Equilibrium, kinetics and thermodynamics studies of lead (II) biosorption on sesame leaf, Bioresources, 7 (2012) 3555–3572.
- [48] J. Biyan, S. Fei, G. Hu, S. Zheng, Q. Zhang, Z. Xu, Adsorption of methyl tert-butyl ether (MTBE) from aqueous solution by porous polymeric adsorbent, J. Hazard. Mater., 161 (2009) 81–87.
- [49] S. Karthikeyan, B. Sivakumar, N. Sivakumar, Film and pore diffusion modeling for adsorption of reactive red 2 from aqueous solution on to activated carbon prepared from biodiesel industrial waste, E-J. Chem., 7 (2010) S175-S184.
- [50] P.K. Dutta, A.K. Ray, V.K. Sharma, F.J. Millero, Adsorption of arsenate and arsenite on titanium dioxide suspensions, J. Colloid Interface Sci., 278 (2004) 270–275.
- [51] B.H. Hameed, Evaluation of papaya seed as a non conventional low cost adsorbent for removal of MB, J. Hazard. Mater., 162 (2009) 939–944.
- [52] D.M. Borrok, J.B. Fein, The impact of ionic strength on the adsorption of protons, Pb, Cd, and Sr onto the surfaces of gram negative bacteria: testing non-electrostatic, diffuse, and triple-layer models, J. Colloid Interface Sci., 286 (2005) 110–126.
- [53] M.H. Salmani, S. Zarei, M.H. Ehrampoush, S. Danaei, Evaluations of pH and high ionic strength solution effect in cadmium removal by zinc oxide nanoparticles, J. Appl. Sci. Environ. Manage., 17 (2013) 583–593.
- [54] S. Lata, P.K. Singh, S.R. Samadder, Regeneration of adsorbents and recovery of heavy metals: a review, Int. J. Environ. Sci. Technol., 12 (2015) 1461–1478.
- [55] M. Liu, Y. Deng, H. Zhan, X. Zhang, Adsorption and Desorption of Copper(II) from solutions on new spherical cellulose adsorbent, J. Appl. Polym. Sci., 84 (2002) 478–485.
- [56] A.R. Ipeaiyeda, G.O. Tesi, Sorption and desorption studies on toxic metals from brewery effluent using eggshell as adsorbent, Adv. Nat. Sci., 7 (2014) 15–24.
- [57] D. Kołodyńska, J. Krukowska, P. Thomas, Comparison of sorption and desorption studies of heavy metal ions from biochar and commercial active carbon, Chem. Eng. J., 307 (2017) 353–363.
- [58] B. Swarup, M. Umesh, Continuous fixed-bed column study and adsorption modeling: removal of lead ion from aqueous solution by charcoal originated from chemical carbonization of rubber wood sawdust, J. Chem., 2015 (2015) 1–9.
- [59] C. Liu, X. Liang, J. Liu, W. Yuan, Desorption of copper ions from the polyamine functionalized adsorbents: behaviors and mechanisms, Adsorpt. Sci. Technol., 34 (2016) 455–468.
- [60] S.H. Chien, W.R. Clayton, Application of elovich equation to the kinetics of phosphate release and sorption in soils, Soil Sci. Soc. Am. J., 44 (1980) 265–268.
- [61] K.E.M.Y. Nasehir, A. Ismail, F.P.M.L. Muhamad, O.S. Bello, M.A. Ahmad, Fixed-bed column study for Cu(II) removal from aqueous solutions using rice husk based activated carbon, Int. J. Eng. Technol. IJET-IJENS, 11 (2011) 186–190.
- [62] J.T. Nwabanne, P.K. Igbokwe, Adsorption performance of packed-bed column for the removal of lead (ii) using oil palm fibre, Int. J. Appl. Sci. Technol., 2 (2012) 106–115.
- [63] Z.C. Zaira, B.A.H. Sharifah, M.Z. Sarifuddin, Evaluating design parameters for breakthrough curve analysis and kinetics of fixed-bed column for Cu(II) cations using lignocellulosic wastes, Bioresources, 10 (2015) 732–749.
- [64] N. Rahman, M.F. Khan, Nitrate removal using poly-o-toluidine zirconium (IV) ethylenediamine as adsorbent: batch and fixed-bed column adsorption modeling, J. Water Process Eng., 9 (2016) 254–266.